

# The Rio Pardo salient, northern Araçuaí orogen: an example of a complex basin-controlled fold-thrust belt curve

Eliza Peixoto<sup>1\*</sup>, Fernando Flecha de Alkmim<sup>1</sup>, Antônio Carlos Pedrosa-Soares<sup>2</sup>

**ABSTRACT:** *The Rio Pardo salient, the large antitaxial curve described by the Araçuaí fold-and-thrust belt along the southeastern edge of the São Francisco craton, is one of the most prominent and one of the least studied features of the Brasiliano Araçuaí-West Congo orogenic system (AWCO). In addition to the Archean/Paleoproterozoic basement, the salient is comprised of metasedimentary rocks mainly from the Neoproterozoic Macaúbas Group and the Salinas Formation. Its western limb occupies a portion of the Espinhaço ridge, where the NS-trending structures of the Araçuaí belt progressively curve NE and E, thereby defining the hinge zone along the Serra Geral on the Minas-Bahia boundary. The eastern limb is NW-trending and marked by a major shear zone. In models postulated to generate the AWCO through the closure of the Neoproterozoic Macaúbas basin, this large curve plays a critical kinematic role. Yet, in spite of this, its development is still not fully understood. How did this curve originate? Which factors controlled its generation? Our field study performed in the northern Araçuaí orogen characterized the kinematic picture of the salient, and led to a model that addresses these questions. The results we obtained indicate that the Rio Pardo salient developed in response to four deformation phases. The contractional D1 and D2 phases are coaxial and responsible for a craton-directed tectonic transport along the salient's outer arc, which is coupled with an overall southward motion of the inner arc, thereby giving rise to a rather complex kinematic picture. Furthermore, structures of the D1/D2 phases define a zigzag pattern with alternating NE- and NW-trending segments along the salient's leading edge. Along the NE-trending segments, the metasedimentary rocks are thrust northwestwards on top of the craton basement, while along the NW-trending segments, the supracrustal rocks are displaced along dextral to reverse-dextral transpressional shear zones located on the basement/cover contact. Structures of the D3 phase, which are well developed in the hinge zone, record a final WSW-ENE contraction, which was responsible for rotation of the preexistent fabric elements around NNW-trending axes and the enhancement of the salient curvature. The D4 phase is extensional and is recorded by two large-scale structures, the Chapada Acauã and Tingui normal shear zones, as well as by the normal-sinistral reactivation of the Itapebi strike-slip shear zone that marks the salient eastern limb. We interpret the initiation of the Rio Pardo salient during the collisional 565-575 Ma D1/D2 phases essentially as a primary arc that is mainly controlled by the geometry of the Macaúbas precursor basin. The thickened internal portion of the Rio Pardo salient was affected by extensional tectonism at c. 530 Ma, and is recorded by the D4 deformation phase, which is currently ascribed to the extensional collapse of the Araçuaí-West Congo orogen.*

**KEYWORDS:** Rio Pardo salient; Araçuaí belt; primary curve; bivergent fold-thrust wedge; extensional collapse.

## INTRODUCTION

The map-view pattern of fold and thrust belts (f-t-belts) is characterized by straight segments and curves of various sizes and shapes currently referred to as salients, recesses, arcs, oroclines, and syntaxis. Salients or antitaxial curves are defined as convex-to-foreland structures. Recesses or syntaxial curves, on the contrary, are concave-to-foreland structures. Extremely pronounced syntaxial curves are called syntaxis.

Salients and recesses, the most common and prominent categories of f-t-belt curves, attracted the attention of researchers already in the first tectonic studies of mountain belts (see Marshak 2004 for a comprehensive review). The interest in f-t-belt curves has persisted over the years, resulting in a robust foundation of knowledge based on their geometric, kinematic and dynamic aspects (e.g., Laubscher 1972, Beutner 1977, Eldredge *et al.* 1985, Marshak & Wilkerson 1992, Macedo & Marshak 1999, Marshak & Flöttmann 1996, Paulsen &

<sup>1</sup>Departamento de Geologia, Escola de Minas, Universidade Federal de Ouro Preto – Ouro Preto (MG), Brazil. E-mails: einpeixoto@gmail.com, ffalkmim@gmail.com

<sup>2</sup>Centro de Pesquisas Professor Manoel Teixeira da Costa, Instituto de Geociências, Universidade Federal de Minas Gerais – Belo Horizonte (MG), Brazil. E-mail: pedrosasoares@gmail.com

\*Corresponding author.

Manuscript ID: 20170134. Received on: 11/14/2017. Approved on: 02/03/2018.

Marshak 1999, Spraggins & Dunne 2002, Gutiérrez-Alonso *et al.* 2004, 2012, Marshak 2004, Weil & Sussman 2004, Tull & Holm 2005, Wilkerson *et al.* 2007, Silva & Oliveira 2009, Williams *et al.* 2009, Pastor-Galán *et al.* 2011, Prasad *et al.* 2011, Rosembaum *et al.* 2012, Chatzaras *et al.* 2013, Weil *et al.* 2013, Whisner *et al.* 2014, White *et al.* 2016, Szaniawski *et al.* 2017). The majority of these studies are based on the critical taper theory of the development of thrust wedges (Davis *et al.* 1983, Boyer 1995).

After examining a large number of f-t-belt curves and simulating their development in sand-box experiments, Macedo and Marshak (1999), Ribeiro (2001) and Marshak (2004) concluded that these features develop under the influence of several distinct factors. Accordingly, three genetic types of curves are distinguished:

- Basin-controlled curves;
- Curves resulting from irregularities in colliding margins;
- Curves generated by other processes.

Basin-controlled curves form in response to along-strike changes in the pre-orogenic features of the basin in which they develop. Variations in the thickness of the basin fill strata, erosion rates, and the amount of plutonism, as well as in the shape and mechanical properties of the detachment surface, are factors that exert major controls on the f-t-belt geometries. The action of indenters, buttresses and other irregularities in the colliding margins can also lead to the generation of curved structures. Other causes for curve formation are the interference of nonparallel orogenic fronts and strike-slip faulting (Marshak 2004).

The kinematics of curve development has been intensively explored by authors devoted to the study of f-t-belts. From a kinematic point of view, f-t-belt curves can be grouped into two basic categories. Primary arcs (Weil & Sussman 2004) (or non-rotational curves, Marshak 2004) involve faults and folds, which begin as curved structures and remain as such during the whole f-t-belt generation process. On the contrary, rotational curves or oroclines consist of structures, which experience a considerable change in their orientation as deformation progresses or during a subsequent tectonic event (Weil & Sussman 2004, Marshak 2004).

The Araçuaí orogen in southeastern Brazil corresponds to the largest portion of the Ediacaran-Cambrian Araçuaí-West Congo orogenic system (AWCO) (Fig. 1), which also encompasses the West Congolian belt on the African continent. Confined to an enclave between the São Francisco and Congo cratons, the AWCO developed through the closure of the Macaúbas basin during the amalgamation of West Gondwana (Pedrosa-Soares *et al.* 2001, Alkmim *et al.* 2006). As indicated by paleogeographic reconstructions, the Macaúbas basin was made up of an oceanic sector — a

branch of the Neoproterozoic Adamastor ocean — and an ensialic domain linked to a system of long-lived intracontinental rift basins represented by the Pirapora, Paramirim, Nyanga, and Sangha aulacogens of the São Francisco and Congo cratons (Pedrosa-Soares *et al.* 1998, 2001, Alkmim *et al.* 2006, 2017, Cruz & Alkmim 2006, Queiroga *et al.* 2007, Reis & Alkmim 2015, Gonçalves *et al.* 2016) (Fig. 1).

The Araçuaí orogen occupies the region located between the São Francisco craton and the eastern Brazilian continental margin (Pedrosa-Soares *et al.* 2001) (Fig. 1). The Rio Pardo salient (Cruz & Alkmim 2006) is a c. 170 km-long antitaxial curve developed in the orogen's ensialic northern sector. As the most prominent structure of the orogen, the Rio Pardo salient culminates in the region where the intracratonic Paramirim aulacogen (Cruz & Alkmim 2006, Alkmim *et al.* 2017) reaches the São Francisco craton boundary (Fig. 1). First recognized by Cordani (1973) as an arc described by the structures of the “Brasiliano cycle” along the Minas/Bahia boundary, the Rio Pardo salient has remained the least investigated portion of the external Araçuaí orogen since then. Deciphering its internal architecture and understanding its kinematic history is, however, crucial for testing the models postulated for the development of the AWCO as a confined orogenic system. Various models have been proposed for the closure of the Macaúbas basin and the generation of the AWCO (see Alkmim *et al.* 2006 for a review). In all of these models, the large curve described by the Araçuaí orogen along the southeastern boundary of the São Francisco craton plays a critical kinematic role. How did the Rio Pardo salient originate? Was its generation governed by attributes of the Macaúbas basin? If so, which pre-orogenic features controlled its development? Was the salient generation coupled with any rotation component? How was the WSW-ENE shortening documented in the intracratonic Paramirim aulacogen accommodated inside the salient? In order to provide answers to these key questions and to contribute to the understanding of the evolution of the Rio Pardo salient and to f-t-belt curves in general, we carried out a field-based structural investigation in the northern Araçuaí orogen, involving the description of c.700 outcrop stations along a 160 km-wide and 340 km-long area (Fig. 1).

In this paper, we present the results of our study. After addressing the geological context and previous investigations on the Rio Pardo salient, we provide a description of its overall architecture, deformation phases and related fabric elements, which is then followed by a discussion on the implications of our data and our interpretations. We conclude by postulating a model for the generation of the Rio Pardo salient in the tectonic scenario of the development of the Araçuaí-West Congo orogenic system.

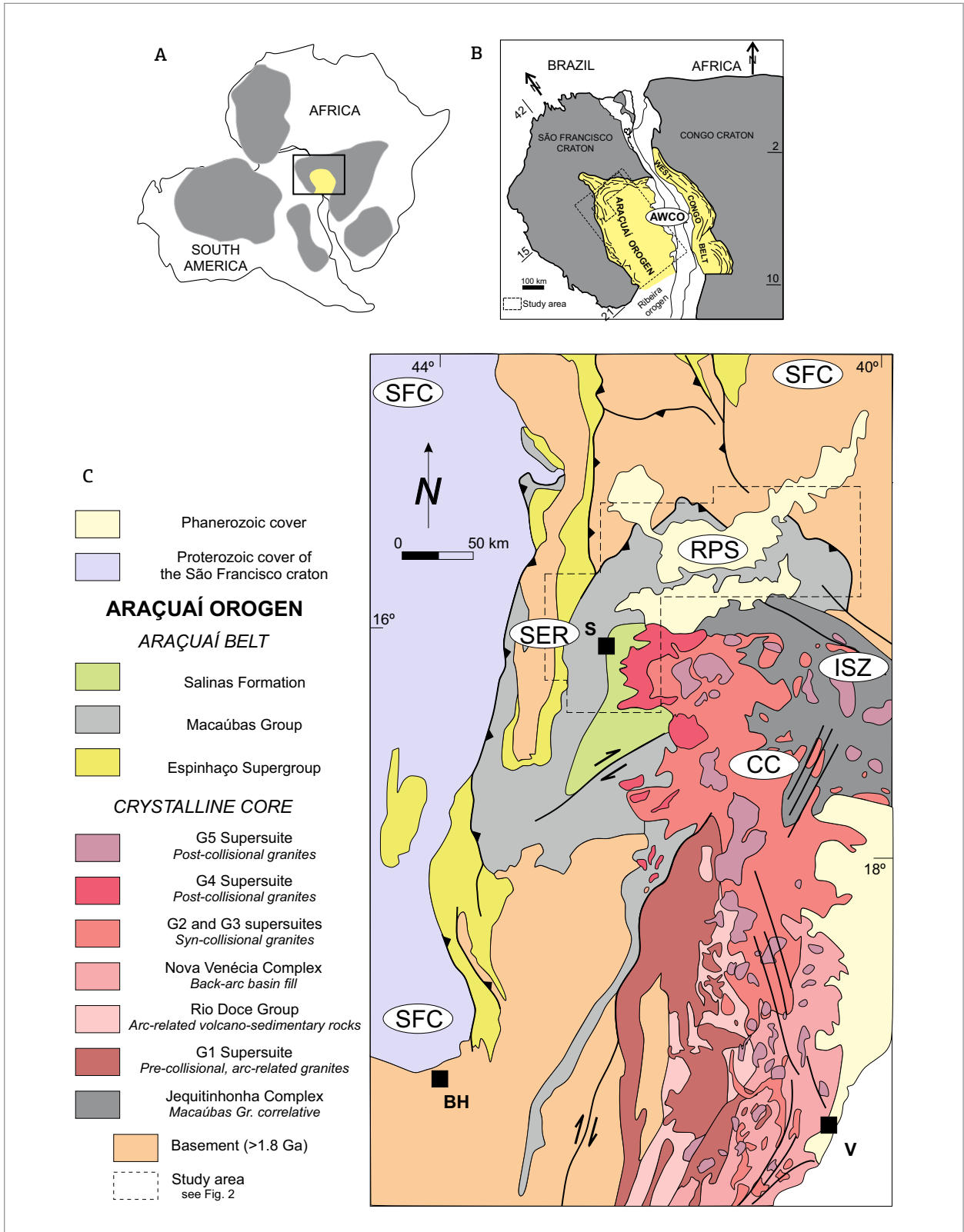


Figure 1. (A, B) The geotectonic setting of the Araçuaí–West Congo orogenic system and the adjoining São Francisco–Congo craton (SFC) in the Gondwanaland context (modified from Alkmim *et al.* 2006). (C) A simplified geologic map of the Araçuaí orogen, highlighting the main lithotectonic assemblages and tectonic compartments (SER, Serra do Espinhaço range fold-and-thrust system, RPS, Rio Pardo salient, ISZ, Itapebi shear zone, CC, crystalline core, SFC, São Francisco craton) (modified from Alkmim *et al.* 2017). Cities: BH, Belo Horizonte; V, Vitória; S, Salinas. The dashed box indicates the location of the study area.

## GEOLOGICAL SETTING

The Araçuaí orogen, or the Brazilian portion of the AWCO, consists of an external f-t-belt, the Araçuaí belt (Almeida 1977), and a crystalline core (Fig. 1). The external f-t-belt involves the Archean/Paleoproterozoic basement and Paleo, Meso and Neoproterozoic metasedimentary rocks metamorphosed under greenschist to amphibolite facies conditions. The crystalline core is made up of amphibolite to granulite facies rocks of the basement and Neoproterozoic supracrustal assemblage in conjunction with five generations of Neoproterozoic granites (Pedrosa-Soares *et al.* 2001, 2008, 2011a, Alkmim *et al.* 2006).

The regional structure known as the Rio Pardo salient (Cruz & Alkmim 2006) dominates the structural picture of the northern Araçuaí orogen. As previously mentioned, Cordani (1973) first demonstrated that the map traces of the Brasiliano structures describe a large arc in northern Minas Gerais. Mapped out by Silva-Filho *et al.* (1974), the salient was later called the Alto do Rio Pardo pericratonic zone by Portela *et al.* (1976). Almeida (1977) defined the Araçuaí belt as the Brasiliano orogenic feature that fringes the São Francisco craton to the east, emphasizing the curvature of its northern segment. Almeida *et al.* (1978) conducted the first stratigraphic, structural and metamorphic investigation into the northern Araçuaí orogen. In this work, the authors detailed the southeast limit of the São Francisco craton, correlated the units of the Araçuaí belt in the region to the Espinhaço Supergroup and the Macaúbas Group, and described the regional metamorphic pattern, which increases southward from the staurolite zone to the K-feldspar/spinel zone. These studies were followed by a series of others, which focused mainly on the stratigraphic framework of the region (e.g., Inda & Barbosa 1978, Uhlein 1991, Barbosa & Dominguez 1996, Pedrosa-Soares *et al.* 2001).

Cruz and Alkmim (2006) portrayed the curvature of the northern Araçuaí belt as a salient, along which the Brasiliano orogenic front interacted with the pre-existent structures of the intracratonic Paramirim aulacogen. The Paramirim aulacogen is a long-living basin filled by the Espinhaço and São Francisco supergroups of the Paleo/Meso- and Neoproterozoic ages, respectively (Danderfer & Dardenne 2002, Cruz & Alkmim 2006, 2007, Cruz *et al.* 2007, Alkmim *et al.* 2006, 2017, Danderfer *et al.* 2009). Extending over the area of the northern Espinhaço ridge and Chapada Diamantina, the aulacogen underwent partial inversion during the Brasiliano event (Cordani 1973, Cruz & Alkmim 2006, Cruz & Alkmim 2007). The sector of maximum inversion strains defines a NNW-oriented deformation zone, currently referred to as the Paramirim Corridor (Alkmim *et al.* 2006). In accordance

with observations by Almeida *et al.* (1978), Cruz and Alkmim (2006) also portrayed the contact between the basement and supracrustal assemblages along the leading edge (the trace of the deformation front) of the salient as a c. 200 m thick, shallow-dipping mylonitic detachment, on which the Araçuaí orogenic front migrated towards the São Francisco craton. They also documented a younger set of NNW-oriented folds and strike-slip shear zones that interfere with older structures, thereby creating the sinuous structural traces of the salient's leading edge and dome-and-basin fold interference patterns.

According to previous mapping projects and stratigraphic correlations (e.g., Inda & Barbosa 1978, Uhlein 1991, Barbosa & Dominguez 1996, Pedrosa-Soares *et al.* 2001, Wosniak *et al.* 2013, Knauer *et al.* 2015) and our own work in the region, the units involved in the Rio Pardo salient are the following (Figs. 1 and 2):

- A basement assemblage made up of units older than 1.8 Ga and represented by the Porteira (Noce *et al.* 2007a, 2007b, Silva *et al.* 2016) and Tingui (Knauer *et al.* 2015, Silva *et al.* 2016) complexes, as well as the Gavião, Itabuna-Salvador-Curaçá and Jequié blocks (Marinho *et al.* 1994, Santos Pinto *et al.* 1998, Barbosa *et al.* 2003, Noce *et al.* 2007a, 2007b, Barbosa *et al.* 2012, Cruz *et al.* 2012a, 2012b, Silva *et al.* 2016);
- The Serra do Inhaúma Group (Lima *et al.* 1981, Uhlein 1991), comprised of a succession of metarhytmite, schist and quartzite. These authors correlate these rocks to the Espinhaço Supergroup deposited between 1.78 and 1.00 Ga (Dussin & Dussin 1995, Martins-Neto 2000, Chemale Jr. *et al.* 2012, Santos *et al.* 2015). This unit is here correlated to the lower Macaúbas Group, as described by Castro (2014), Kuchenbecker *et al.* (2015) and Costa & Danderfer (2017);
- Mafic intrusive, probable correlative of the Pedro Lessa Suite dated at c. 900 Ma (Machado *et al.* 1989, Dussin & Dussin 1995);
- The 875 Ma Salto da Divisa anorogenic suite, composed of sieno- to monzogranites (Moraes-Filho & Lima 2007, Paixão & Perrela 2004, Silva *et al.* 2008);
- The Macaúbas Group and its correlative, the Jequitinhonha Complex. The first unit is comprised of a glacially influenced rift to a passive margin succession accumulated between ca. 850 and 600 Ma (Noce *et al.* 1997, Uhlein *et al.* 1999, 2007, Danderfer & Dardenne 2002, Pedrosa-Soares & Alkmim 2011, Pedrosa-Soares *et al.* 2011a, Babinski *et al.* 2012, Kuchenbecker *et al.* 2015, Costa & Danderfer 2017). The Jequitinhonha Complex consists mainly of Al-rich paragneisses (Pedrosa-Soares *et al.* 2001, 2007, Sampaio *et al.* 2004, Gonçalves-Dias *et al.* 2011, 2016);

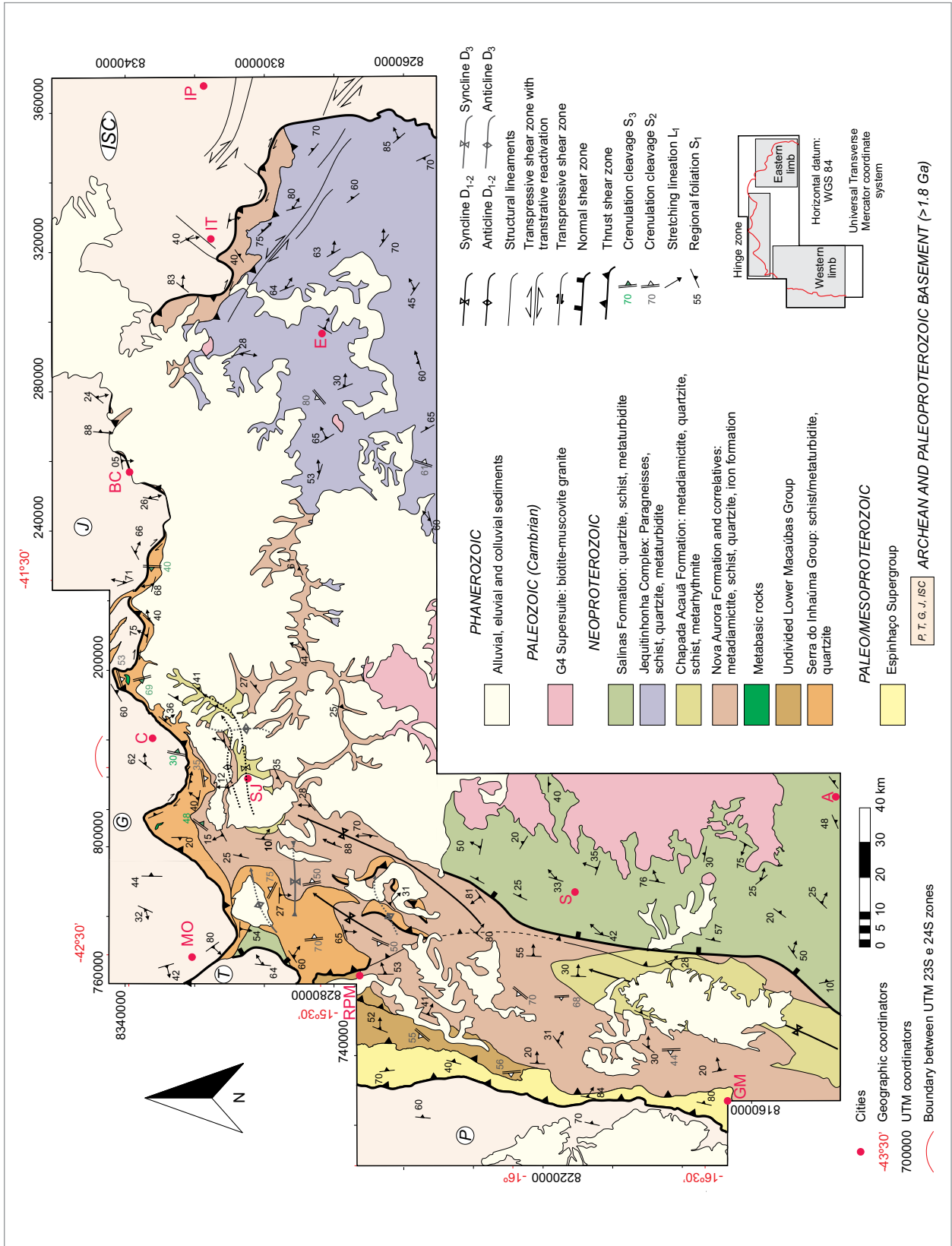


Figure 2. A geologic map of the study area, based on Grossi-Sad et al. (1997), Pinto et al. (2001), Sampaio et al. (2002), Paes et al. (2010). Cities: A, Araçuaí; GM, Grão Mogol; S, Salinas; RPM, Rio Pardo de Minas; MO, Mortugaba; SJ, São João do Paraíso; C, Cordeiros; BC, Belo Campo; E, Encruzilhada; IT, Itambé; IP, Itapetinga. Basement blocks: ISC, Itabuna-Salvador-Curaçá; J, Jequié; G, Gavião; P, Porteirinha Complex; T, Tingui Complex.

- Syn-collisional granites of the G2 and G3 supersuites dated between 585 to 545 Ma (Pedrosa-Soares *et al.* 2001, 2011b, Gradim *et al.* 2014, Peixoto *et al.* 2015, Melo *et al.* 2017a, 2017b);
- The syn-orogenic Salinas Formation, composed of turbiditic metasediments, schists and metaconglomerates with a maximum depositional age of c. 580 Ma (Alkmim *et al.* 2017, Lima *et al.* 2002, Santos *et al.* 2009);
- Late- to post-collisional 530 Ma to 480 Ma granites of the G4 and G5 supersuites (De Campos *et al.* 2004, 2016, Pedrosa-Soares & Wiedmann-Leonardos 2000, Pedrosa-Soares *et al.* 2007).

The stratigraphic succession and the lithological content of the units listed above vary considerably along the salient, as illustrated by Figure 3.

### TECTONIC FRAMEWORK OF THE RIO PARDO SALIENT

The map traces of f-t-belt curves resemble the pattern defined by the trend lines of folds in the profile. With this analogy in mind, Macedo and Marshak (1999) adopted the vocabulary currently used for folds in the description of salients. According to this terminology, the Rio Pardo salient exhibits a moderate hinge zone and two relatively long limbs, a western NS-trending one and an eastern NW-oriented one. Together, these elements define a NNW-oriented mid line and a quite sinuous trend-line pattern, which describe a curvilinear trajectory through the region of the towns Grão Mogol, Cordeiros, and Itambé (Fig. 4).

As one of the most remarkable features of the Rio Pardo salient, its limbs do not encompass the leading edge of the

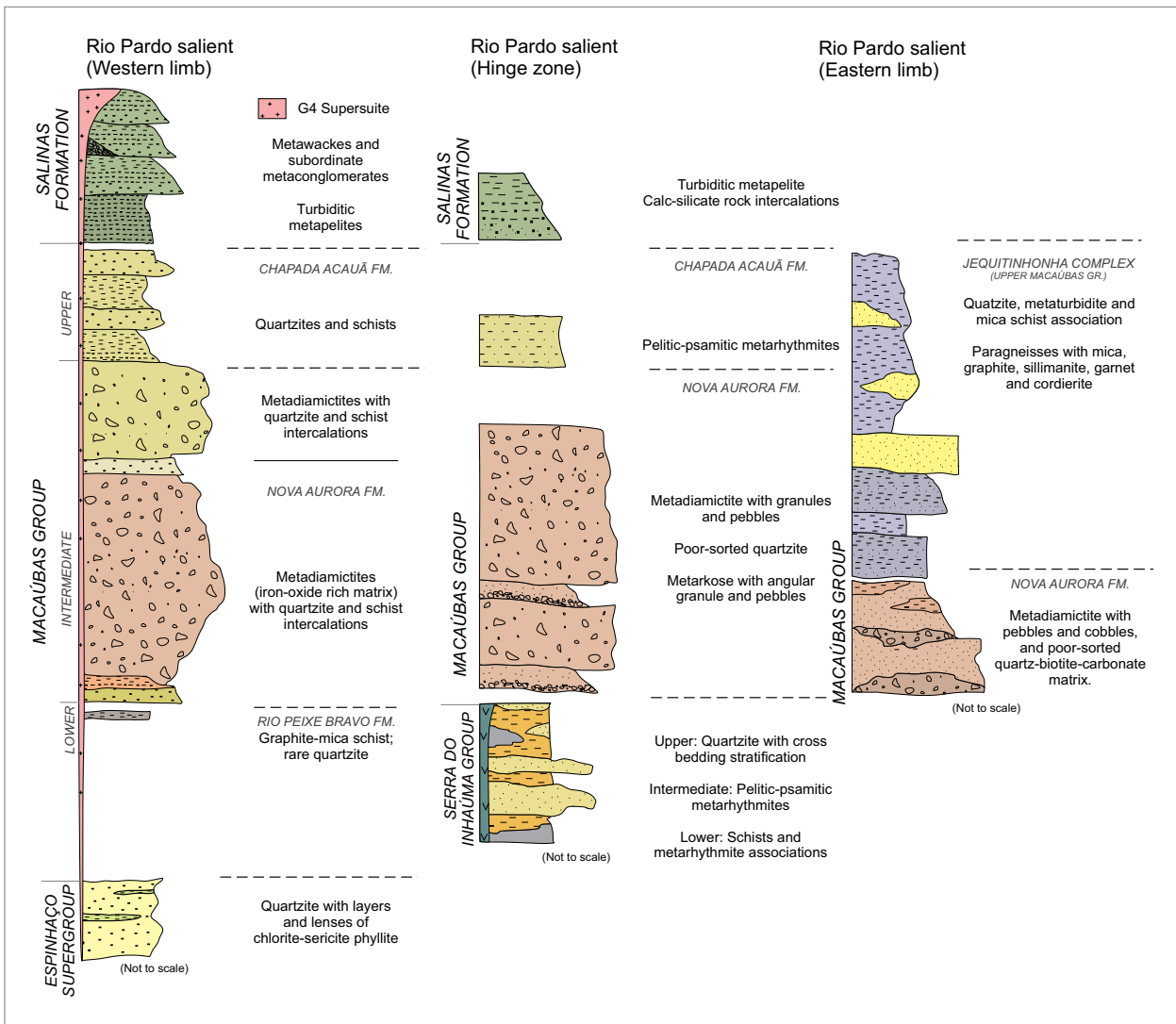


Figure 3. The stratigraphic column for the supracrustal units and intrusive rocks of the study area, emphasizing the correlation between the units throughout the Rio Pardo salient.

northwestern Araçuaí *f-t*-belt along the boundary to the São Francisco craton. The system of folds and thrusts that characterizes the more external portion of the Araçuaí belt continues further north into the craton interior as the western and eastern Paramirim deformation corridor (Fig. 1).

Our detailed structural analysis revealed that the tectonic structures affecting the supracrustal units along the Rio Pardo salient nucleated in the course of four deformation phases, here referred to as the  $D_1$ ,  $D_2$ ,  $D_3$  and  $D_4$  phases. The  $D_1$  phase is characterized by a family of structures ( $F_1$  folds,  $S_1$  foliation,  $L_1$  stretching lineation and ductile shear zones and thrust faults) that record a systematic tectonic motion towards the São Francisco craton. Elements of the  $D_2$  phase ( $F_2$  folds associated with a crenulation cleavage,  $S_2$ ) are also ubiquitous and co-axial to the structures of the  $D_1$  phase. The  $D_3$  phase, detected only along the salient hinge zone, is recorded mainly by regional NNW-trending folds. The fabric elements of the  $D_4$  phase are comprised of a series of extensional structures, such as large-scale normal-sense ductile shear zones and normal faults of varying orientations. In the following sections, we describe the geological architecture of the various sectors of the salient, exploring the kinematic significance of their fabric elements.

### The western limb

The western limb (Fig. 5) encompasses the eastern portion of the Espinhaço ridge and the adjacent Jequitinhonha river valley in northern Minas Gerais. In this part of the salient, only structures from the  $D_1$ ,  $D_2$  and  $D_4$  phases were observed. They occur in association with three regional and roughly NS-trending structures, namely, the eastern half of the southern Espinhaço range fold-thrust system (SER-thrust system), the Chapada Acauã normal shear zone (CASZ), and the Salinas synclinorium (Alkmim *et al.* 2006, 2017, Marshak *et al.* 2006, Santos *et al.* 2009, Peixoto *et al.* 2018, Fig. 5). In addition to the Archean/Paleoproterozoic gneisses

and granitoids, the metasedimentary units affected by these structures include quartzites and phyllites of the Espinhaço Supergroup, a thick succession of the Macaúbas Group, and the metaturbidites of the Salinas Formation, locally cut by granites of the G4 Supersuite (Dussin & Dussin 1995, Pedrosa-Soares *et al.* 2001, 2008, 2011a, Lima *et al.* 2002, De Campos *et al.* 2004, 2016, Santos *et al.* 2009, Kuchenbecker *et al.* 2015) (Figs. 3 and 5).

The fabric elements of the SER-thrust system are manifestations of the coaxial and progressive deformation phases  $D_1$  and  $D_2$ . The most conspicuous structures of the system are the NS-trending thrusts, the reverse faults, the isoclinal to close  $F_1$  folds, the associated axial plane  $S_1$  schistosity, as well as the  $L_1$  stretching lineation (Figs. 5, 6A, 6B and 6C). The  $F_1$  folds, which are W-vergent and kinematic indicators associated with the older  $D_1$  structures attest to a systematic W-directed sense of shear (Figs. 6A and 6B).  $L_1$  stretching lineation is usually on the dip of  $S_1$  foliation. Especially in the more ductile rocks, the  $D_1$  structures are overprinted by the elements of the  $D_2$  phase, which is comprised of near upright, open to close  $F_2$  folds. A vertical crenulation cleavage ( $S_2$ ) (Fig. 6C) occupies the axial plane position of the  $F_2$  folds. All of these elements have been previously described by different authors as the dominant Brasiliano structures of various sectors of the southern Espinhaço ridge fold and thrust system (e.g., Dussin & Dussin 1995, Uhlein *et al.* 1998, Marshak *et al.* 2006).

The CASZ is a large-scale, ESE-dipping, normal sense shear zone that affects rocks of the Upper Macaúbas Group and the base of the Salinas Formation over a c. 40 km-wide and 100 km-long area (Fig. 5). The characteristic elements of the CASZ are ESE-verging fold trains ( $F_4$ ), whose enveloping surfaces also dip ESE. They overprint the  $D_1$  and  $D_2$  structures and are associated with a well-developed WNW-dipping  $S_4$  crenulation cleavage (Fig. 6D). Other structures commonly observed within the CASZ are WNW-dipping antithetic normal faults (Fig. 6E), vertical tension gashes, and ESE-dipping detachments. All together the fabric elements of the CASZ characterize the  $D_4$  deformation phase, which is interpreted as a manifestation of the extensional collapse of the AWCO (Peres *et al.* 2004, Alkmim *et al.* 2006, Marshak *et al.* 2006).

The Salinas synclinorium (or the Salinas fold zone, Alkmim *et al.* 2006, Santos *et al.* 2009) occurs in the hanging wall of the CASZ and is bounded to the east by post-collisional granite intrusions. Within the synclinorium, a system of W to NW verging folds of various sizes and thrust shear zones affect the metaturbidites of the Salinas Formation with increasing intensity towards the east. However, the Salinas metaturbidites are practically undeformed along a synclinorium hinge zone. The regionally penetrative  $S_1$  foliation is only weakly developed in this domain.

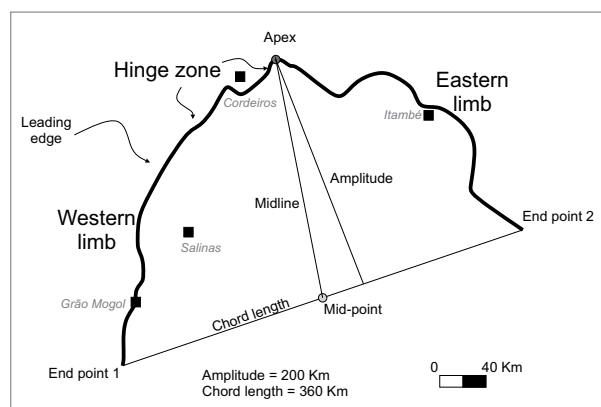


**Figure 4.** Geometric elements of the Rio Pardo salient following the description of Macedo & Marshak (1999).

The metasedimentary rocks involved in the western limb record two metamorphic events. A Barrovian metamorphism assisted the  $D_1$  deformation phase with  $P$ - $T$

conditions increasing eastwards along the SER-thrust system, and reaching  $\sim 8.5$  kbar at  $\sim 650^\circ\text{C}$  (Peixoto *et al.* 2018). Age determinations on the monazite indicated that this event

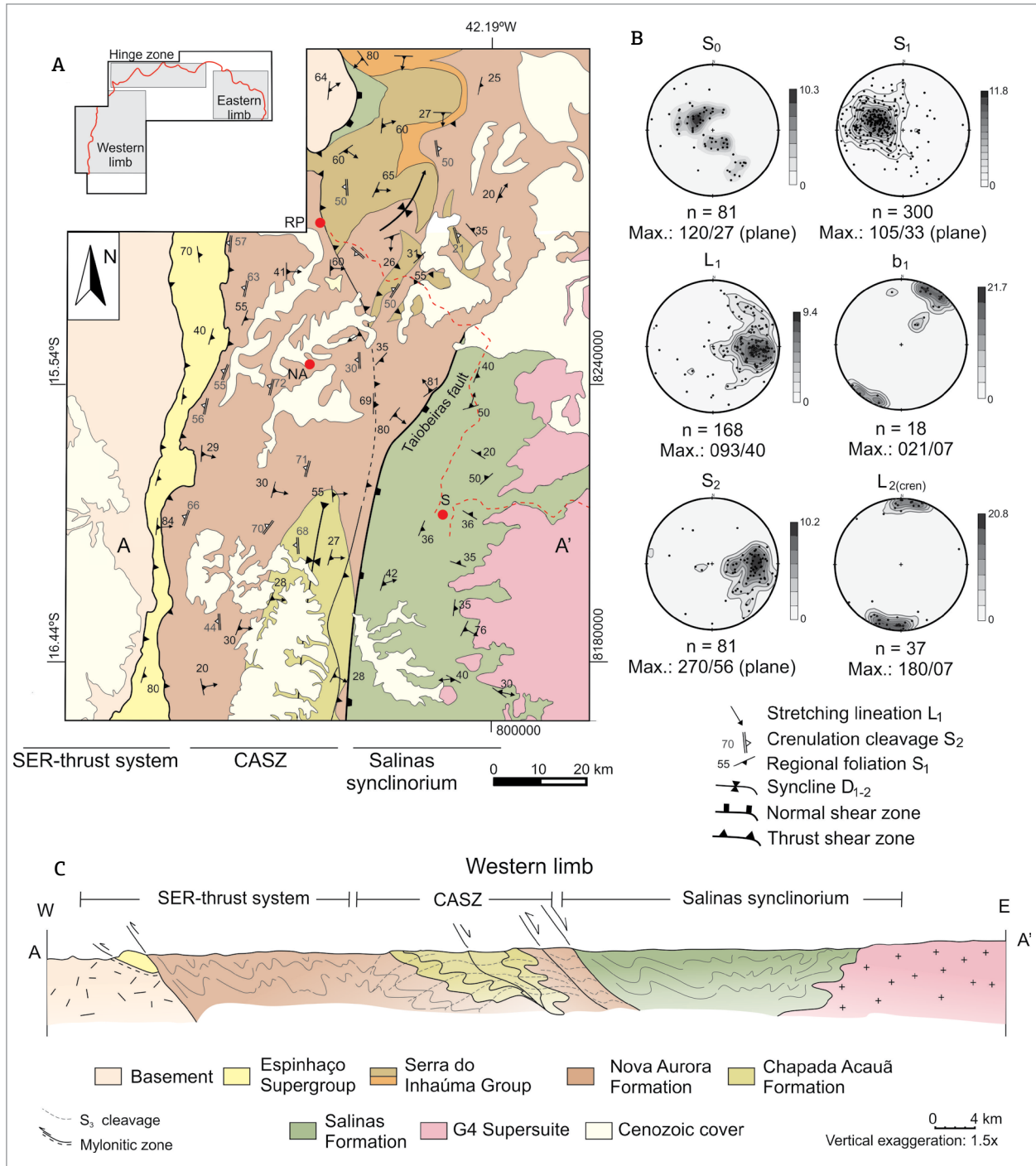


Figure 5. (A) A geologic map of the western limb of the Rio Pardo salient, showing the main regional structures: SER-thrust system, Southern Espinhaço range fold-thrust system; CASZ, Chapada Acauã normal shear zone; and Salinas synclinorium. (B) The equally synoptic contoured area plots of the associated main, small-scale fabric elements.  $S_0$ : poles to bedding;  $S_1$ : poles to main foliation;  $L_1$ : stretching lineation;  $b_1$ : hinges of the  $F_1$  folds;  $S_2$ : poles to the  $D_2$  crenulation cleavage;  $L_{2(cren)}$ : crenulation lineation ( $D_2$ ). (C) The cross-section shows structures of collisional stage ( $D_1$ ) overprinted by CASZ ESE-verging fold trains generated during the  $D_4$  extensional phase. Rocks of the Salinas Formation in the hanging wall of the CASZ configure a synformal structure generated during  $D_1$ . Cities: S, Salinas; NA, Nova Aurora; RP, Rio Pardo de Minas.

took place between 575 and 565 Ma. A second low pressure metamorphic event (Buchan-type) is recorded in the eastern half of the western limb. It took place under 3 to 5.5 kbar and up to 640°C at around 530 Ma (Peixoto *et al.* 2018).

### The hinge zone

The hinge zone, extending over the Serra Geral and Rio Pardo river valley, is the largest and by far the most complex sector of the salient (Fig. 7). A large portion of the sector is covered by Cenozoic sediments and exposures that are predominantly of the Macaúbas Group and correlative units. Occurrences of the Serra da Inhaúma Group are restricted to the southwestern end of the hinge zone and a narrow strip along its leading edge. The salient nucleus is occupied by a large volume of granitic intrusions of the G2 (syn-collisional), G4 and G5 (post-collisional) Supersuites (Pedrosa-Soares *et al.* 2001, 2011b, De Campos *et al.* 2004, 2016, Silva *et al.* 2011, Peixoto *et al.* 2018).

The structures of all the deformation phases occur in the hinge zone. The orientation of the dominant and co-axial  $D_1$  and  $D_2$  structures varies from place to place, giving

rise to sinuous trend lines in the leading edge and internal portion of the salient (Fig. 7). These changes in orientation result basically from:

- changes in orientation of the basement-cover contact along the leading edge;
- folding of the  $D_1/D_2$  structures around NNW-oriented  $F_3$  axes.

The structural traces of the dominant  $D_1$  and  $D_2$  structures along the leading edge of the hinge zone have a zigzag pattern in map-view. They consist of alternating NE- and NW-trending segments (Figs. 7, 8 and 9). Along the N40-60°E-trending segments (sectors I, II, III, Figs. 7 and 8) the metasedimentary rocks are thrust toward the northwest, on top of the basement (Figs. 10A and 10B), while along the N40-60°W-trending segments (sectors IV, V VI) they are displaced along dextral to reverse-dextral transpressional shear zones (Figs. 7, 8 and 9).

Another remarkable feature of this domain is the vergence reversal of the  $D_1/D_2$  in the inner arc of the salient



Figure 6. Structures of the western limb of the Rio Pardo salient: (A) W-verging  $F_1$  open fold and the associated  $S_2$  axial plane foliation affecting metasandstones of the Espinhaço Supergroup. (B) Stretched clast of a Macaúbas Group metadiamicite. The sigmoidal shape of the clast and enveloping  $S_1$  foliation attest to the reverse, top-to-the-west sense of shear. (C) Symmetric vertical  $S_2$  crenulation cleavage, affecting a micaschist of the Macaúbas Group. (D) Prominent NW-dipping  $S_4$  cleavage in metadiamicite of the Macaúbas Group. (E) Outcrop-scale antithetic normal fault of the  $D_4$  extensional phase cutting metapelites of the Macaúbas Group.

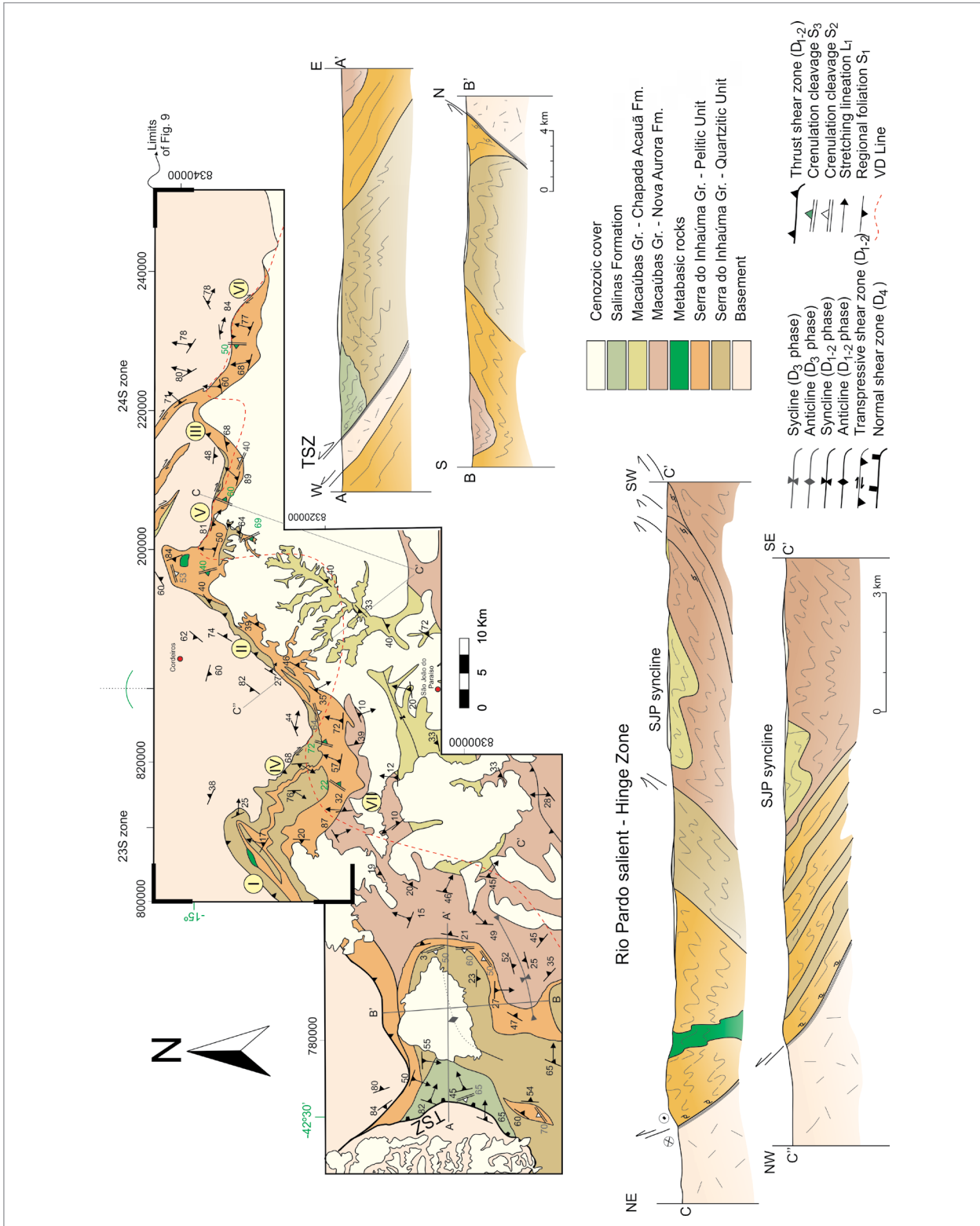


Figure 7. A geologic map of the Rio Pardo salient hinge zone, showing the main regional structures. The A-A' cross-section, on the western portion of the area, shows the normal-sense Tingui shear zone (TSZ). The B-B' cross-section, perpendicular to A-A', shows structures with reverse top-up-to-the north vergence. Respective A-A' and B-B' outcrop-scale structures pictures are shown in Figure 11. The C-C' cross-section represents the NW-trending segments of the hinge zone; see Figure 8 (stereograms V), Figure 9 and Figure 10 (outcrop scale structures). The C'-C'' cross-section shows the NE-trending segments; see Figures 8 (stereogram II), 9 and 10. The Chapada Acauá Formation occurs on the São João do Paraíso syncline (SJP syncline). The vergence divisor line (VD-line) shows structures vergence changing in the region of D<sub>1</sub>/D<sub>2</sub>.

(sector VII, Fig. 7). The vergence north of the VD-line shown in the map of Figure 7 is directed to the São Francisco craton, while south of the VD-line, the dominant structures verge toward the orogen interior (Figs. 10C and 10D), thus characterizing a double fold-thrust wedge (Fig. 7). Except for the change in orientation and vergence, the  $D_1$  structures exhibit (in this part of the salient) the same characteristics as in the western limb. They are especially well developed and exposed in NE-trending sectors of the leading edge (Fig. 7), where the basal detachment is represented by a mylonitic shear zone orientated at 120/33 (Figs. 7, 8, 10A and 10B). The  $F_1$  folds in the metasedimentary rocks are tight to isoclinal and NW-verging. The  $S_1$  schistosity, always associated with a down-dip stretching lineation, shows the preferred orientation 120/33 (Figs. 7 and 8). The  $L_1$  stretching lineation and the associated kinematic indicators, such as rotated porphyroclasts and foliation pods attest to a top-up-to-northwest dominant motion.

The imprint of the  $D_2$  phase is not as homogenous as that of the  $D_1$  phase, as it varies strongly with lithotype and location. The  $F_2$  folds are of regional scale and usually open to tight and upright. They show a pronounced asymmetry and south vergence in the inner portion of the salient. The associated  $S_2$  crenulation cleavage is well developed and often transposes the  $S_1$  foliation in schists and micaceous quartzites. In many localities, the  $S_2$  cleavage appears as the most prominent small-scale structure.

The  $D_3$  phase is recorded throughout the whole domain by NNW-trending folds of variable scale, and is always associated with the  $S_3$  crenulation cleavage. Folds of this phase overprint preexistent  $D_1/D_2$  folds, giving rise to dome-and-basin and locally very complex interference patterns.

The CASZ, the main regional  $D_4$  structure, progressively curves NE in the northern end of the western limb and becomes covered by Cenozoic sediments in the internal portion of the hinge zone. As shown in the map of Figure 7, we inferred the continuation of the CASZ beneath this cover and its connection with the strike-slip system that marks the eastern limb (see the following section). In the outer arc of the salient, the manifestation of the  $D_4$  phase is represented by a normal-sense shear zone developed along the contact between the Salinas Formation and the basement assemblage in the northwestern end of the domain (the Tingui shear zone, TSZ). Characterized by phylonites and mylonites, this shear zone (Figs. 7 and 11) shows S-C foliations and asymmetric  $\sigma$ -type feldspar porphyroclasts, which indicate a top-down-to-the-east motion (Figs. 11B and 11C).

Two metamorphic events are recorded in the hinge zone. A Barrovian metamorphism assisted  $D_1$  and  $D_2$  deformation phases, with P-T conditions increasing toward the north, reaching -7 kbar and -660°C in the kyanite zone. Monazite dating in this region indicates that the metamorphic peak

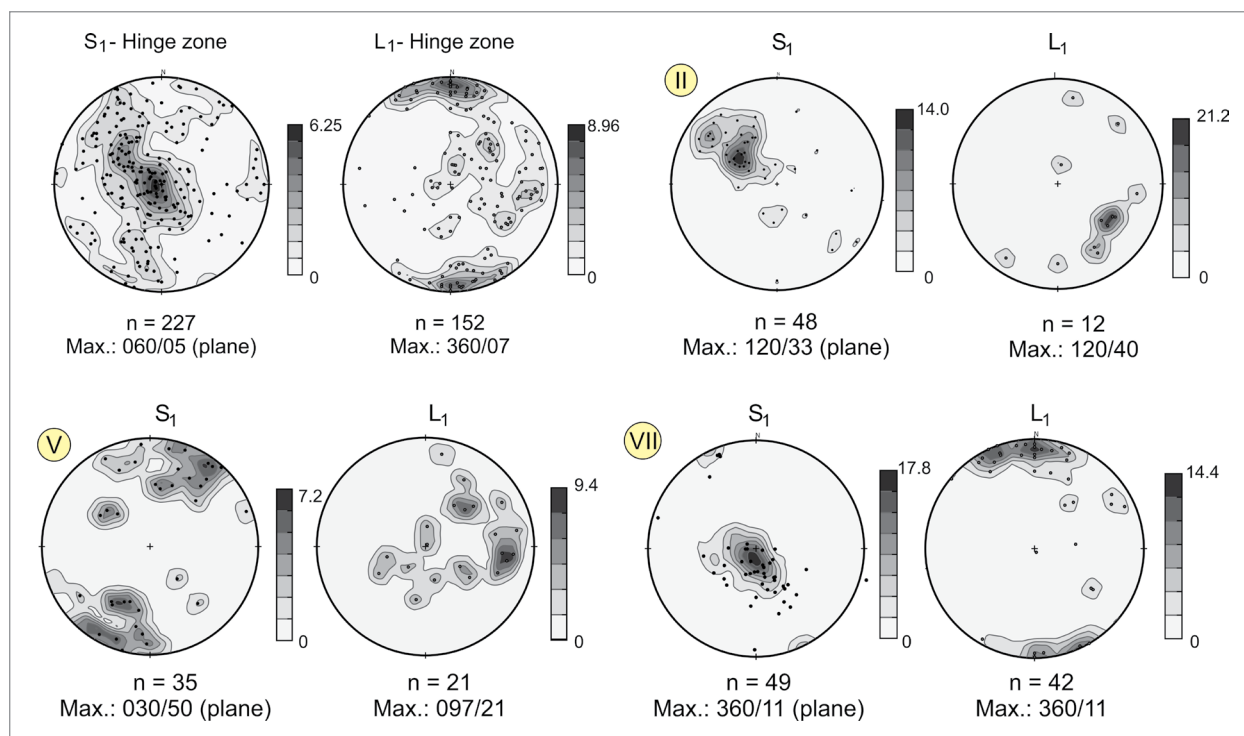


Figure 8. Equally synoptic contoured area plots of regional  $S_1$  foliation and associated  $L_1$  stretching lineation in the hinge zone. NE-trending and NW-trending segments are represented by the segments II and V. The inner portion with a southward vergence is represented by the stereogram of region VII (see Fig. 7).

of this event was reached at c. 562 Ma. A second event at around 525 Ma is also recorded in monazite grains. A later resetting is dated at c. 505 Ma. A clockwise PT trajectory is deduced for this region through textural and mineralogical relationships (Peixoto 2017).

### The eastern limb

The eastern limb of the salient occupies the area located between the towns of Belo Campo and Encruzilhada, extending between the eastern end of the Serra Geral and the Rio Pardo river valley (Figs. 2 and 12). Shaped by the NW-trending dextral Itapebi shear zone (Corrêa-Gomes 2000, Sampaio *et al.* 2004, Alkmim *et al.* 2006, Cruz *et al.* 2012a) (Fig. 12), the eastern limb is marked by a sub-regional positive flower structure generated during the  $D_1$

phase, which affects the basement, 880 Ma Salto da Divisa Suite, and the Macaúbas Group.

The tectonic framework of this portion of the salient resembles the NW-trending segments of the hinge zone in many ways. Along the leading edge, rocks of the Macaúbas Group are thrust on top or are juxtaposed with basement rocks along reverse dextral shear zones. Basement gneisses in this region are mylonitic, exhibiting a variety of kinematic indicators, such as rotated porphyroclasts, asymmetric boudins and S-C foliation. The  $S_1$  foliation shows variable dips across the zones and root in the vertical stem of the flower structure, which is illustrated by upright and tight to isoclinal  $F_1$  folds (Figs. 13A, 13B and 13C). The southwestern branch of the structure is characterized by a dominant top-up-to-SW vergence and secondary transpressive shear

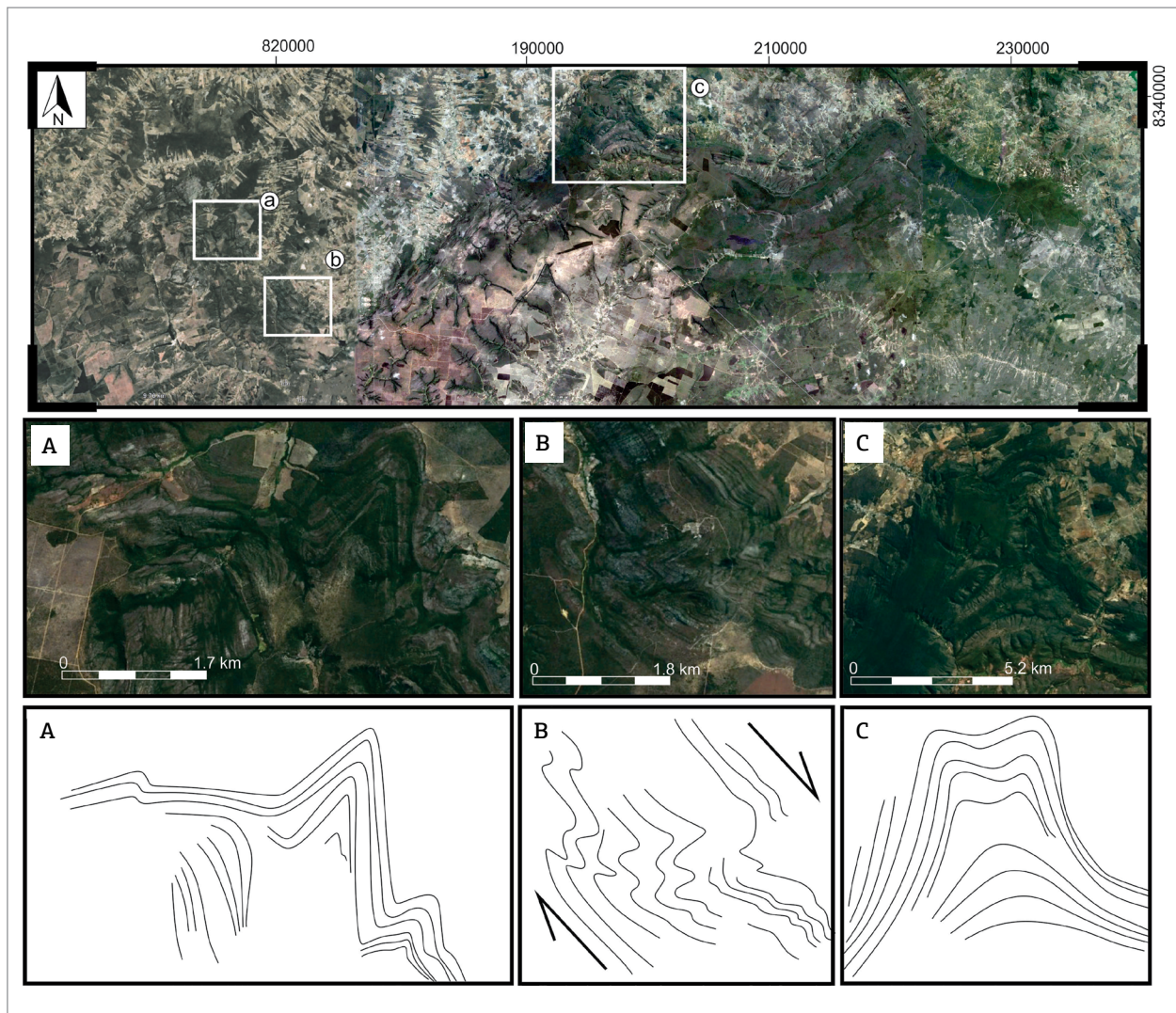


Figure 9. A satellite image of the Rio Pardo salient hinge zone (see location in Fig. 7) and sub-regional associated folds. The NE-trending segments show straight map-view structural traces (reflecting thrusting contact), while the NW-trending segments folds reflect the dextral component of deformation. M-type folds with a N-S axis occur between the segments and may represent  $D_2$  final shortening.

zones (Fig. 12). The  $L_1$  stretching lineation plunges preferentially SE, showing, however, significant variations.

$D_2$  fabric elements were rarely observed. Some NW-trending open folds affect the  $S_1$  foliation in the region (Fig. 13D), which is also locally folded around the NS-oriented axes of the  $F_3$ -folds. In many places along the domain, sinistral

and normal reactivations of the Itabebi system have been observed as previously documented by Alkmim *et al.* (2006). The sinistral motions can be associated with the  $D_3$  shortening, whereas the normal sinistral motion probably resulted from the SE-down motion along the CSAZ during the  $D_4$  extensional phase.

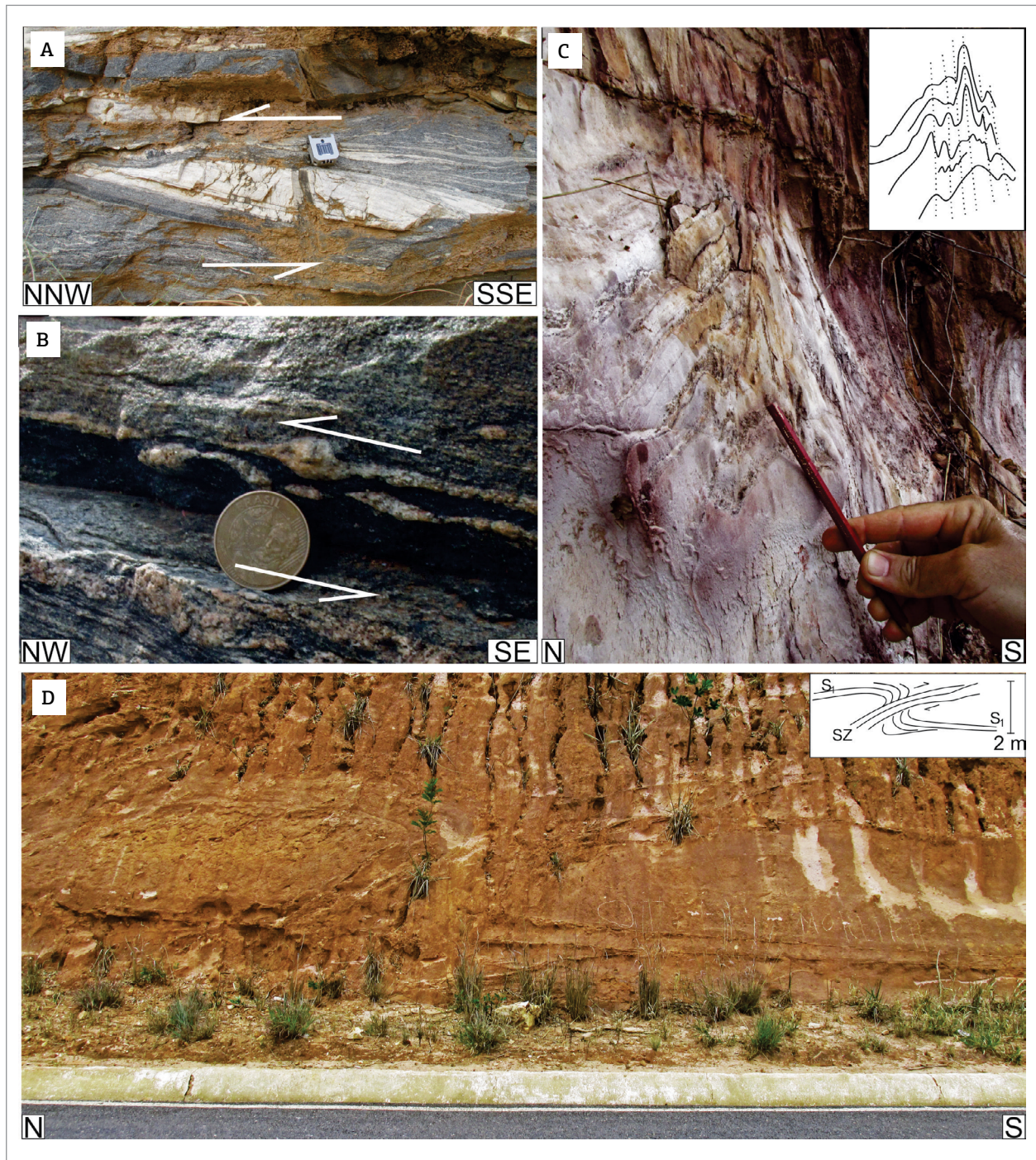


Figure 10. Structures of the Rio Pardo salient hinge zone: (A, B) Structures of the shallow-dipping detachment on the NE-trending segments. Sigmoidal quartz-feldspatic band and sigmoidal feldspar porphyroclast of Gavião Block gneiss, attesting to the reverse, top-to-the-northwest sense of shear. (C) Location of vergence changing, with upright folds and related subvertical  $S_1$  foliation; (D) back-thrusting verging southward.

The  $D_1$  and  $D_2$  phases are associated with the peak of the regional metamorphism, which is characterized by amphibolite to granulite-facies assemblages in the region (Peixoto 2017).

### An integrated kinematic picture of the Rio Pardo Salient

Traces of  $S_1$  foliation (shown in Fig. 14) describe the large arc of the Rio Pardo salient. The motion picture of the metasedimentary rocks during the  $D_1$  principal deformation across the salient can be visualized in the map in Figure 14, which was made by plotting and extrapolating the trend of the  $L_1$  stretching lineation and the associated sense of shear (indicated by the arrows). It is clear from this map that motion toward the foreland predominates in the western limb and out of the arc of the salient, whereas in the inner arc, the flow trajectories are toward the south and southwest.

## DISCUSSION

### Significance of the deformation phases

To unravel the tectonic significance of the deformation phases documented in the limbs and hinge zone of the salient, we start by examining the  $D_1$  and  $D_2$  structures

in the western limb, where they were previously investigated by various authors. As the dominant fabric elements of the external Araçuaí orogen, the  $D_1/D_2$  structures record the Brasiliano event in the region, which is in turn viewed as a product of a general E-W contraction (Pedrosa-Soares *et al.* 2001, Alkmim *et al.* 2006). The Barrovian metamorphism syn-kinematic to  $D_1$  was recently dated in this region between 575 and 565 Ma (Peixoto *et al.* 2018), the age interval of the collisional stage of the Araçuaí orogen (Pedrosa-Soares *et al.* 2001, 2008, 2011b).

Keeping the same attributes and crosscut relationships of the western limb, the  $D_1/D_2$  folds and thrusts progressively curve toward the NE and enter the hinge zone, where they exhibit considerable variations in orientation and form a double-verging deformation wedge. Along the leading edge of the hinge zone, these structures preserve the foreland-directed vergence, as previously documented by Cordani (1973), Almeida *et al.* (1978), Uhlein (1991) and Cruz and Alkmim (2006). They change their character in the eastern limb, and are represented by the dextral reversal Itapebi shear zone. This fact implies that the salient as whole is delineated by the Brasiliano  $D_1/D_2$  collisional structures, and regardless of later modifications, its initial development was coupled to a quite complex flow pattern, as illustrated by Figure 14.

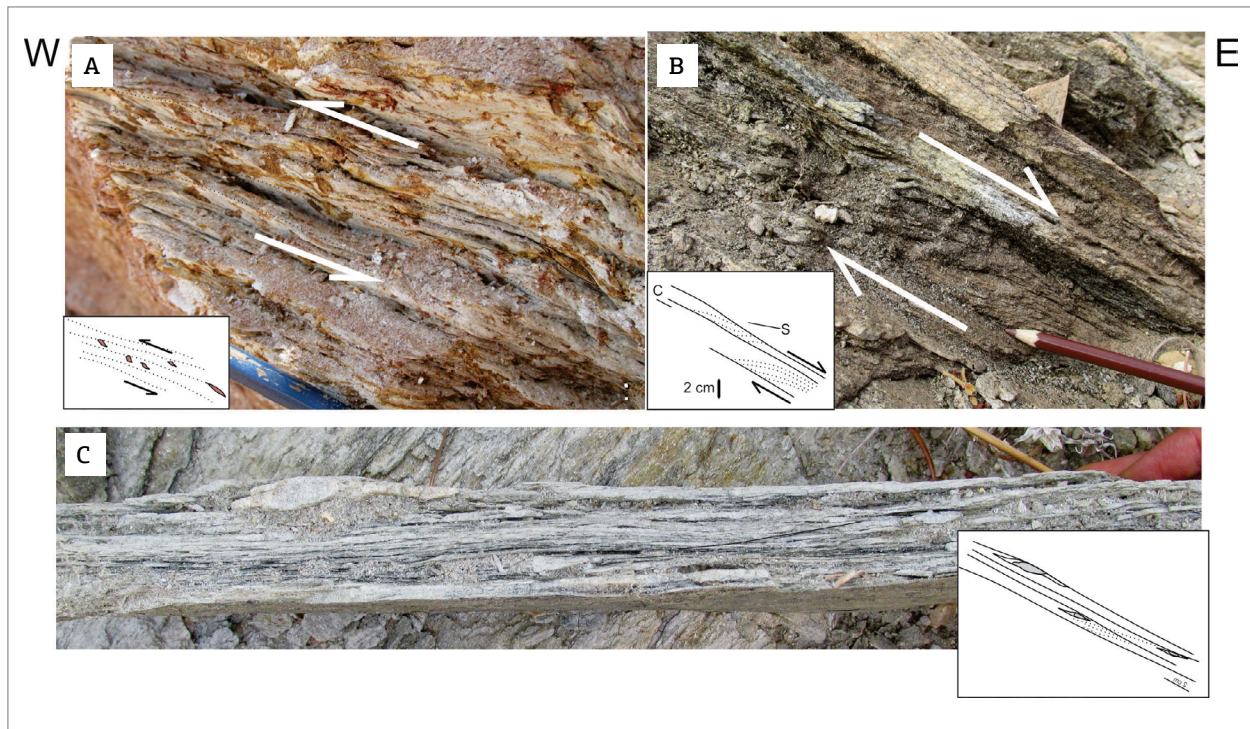


Figure 11. Collisional and collapse structures of the Rio Pardo salient on the Tingui shear zone (see Figure 7), western region of the hinge zone. (A) Garnet porphyroblasts attesting reverse, top-to-the-west vergence. (B, C) Mylonite and phyllonite with S-C foliation and feldspar porphyroblast showing normal, top-down-to-the-east sense of shear.

The remarkable zigzag map pattern described by the  $D_1/D_2$  structures along the outer arc of the hinge zone could result from:

- the generation of an ENE trending hinge zone and, later, folding around the NNW-trending  $F_3$  axes;
- the generation of an ENE trending hinge zone and subsequent displacement along a system of NW-trending dextral strike-slip shear zones;

- the propagation of the deformation front against an irregular-shaped basement high and consequent partition of the strain along ENE-oriented frontal ramps and NW-trend lateral obstacles;
- a combination of these processes.

Our data indicated that this pattern more likely resulted from a combination of these mechanisms, for the

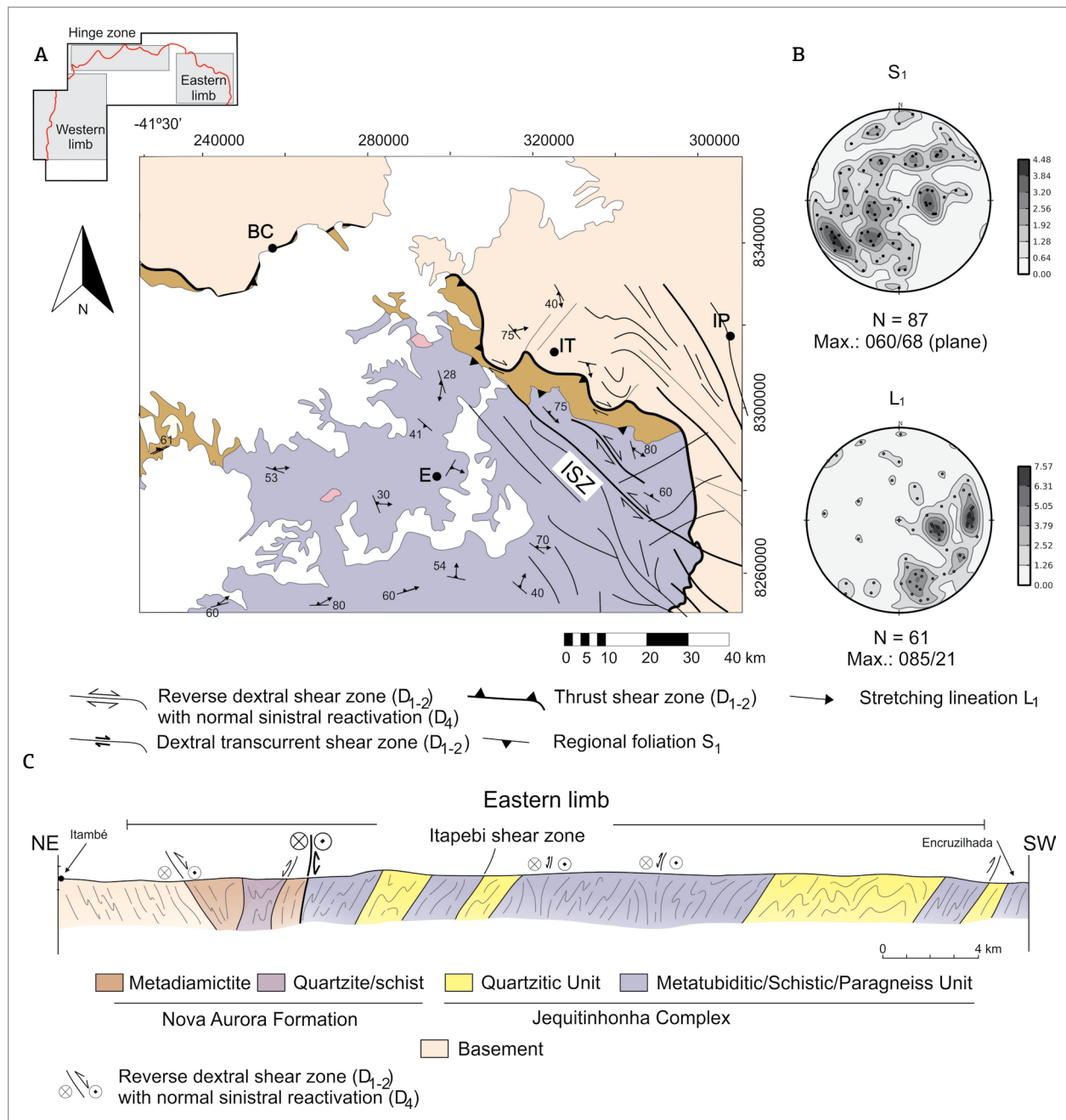


Figure 12. (A) A geologic map of the Rio Pardo salient eastern limb (ISZ, Itapebi shear zone). (B) Equally synoptic contoured area plots of the regional  $S_1$  foliation and associated  $L_1$  lineation. (C) The area is affected by a dextral transpressional shear zone reactivated by a sinistral-normal shear sense. The overall scenario reflects a positive flower structure, with the main stem passing along the Nova Aurora Formation and the Jequitinhonha Complex (juxtaposed by a structural contact). E: Encruzilhada; IT: Itambé; BC: Belo Campo; IP: Itapetinga.

following reasons. As previously mentioned, the  $F_3$  folding affected the hinge zone, and represents an important mechanism for the generation of the sinuous map traces of  $D_1/D_2$  structures, as emphasized by Almeida *et al.* (1978) and Cruz and Alkmim (2006). However, this process alone cannot explain the strike-slip motions observed along the NW-oriented segments of the leading edge. On the other hand, at least in the western part of the leading edge, there is no clear evidence for offsets of basement and cover structures along the NW-trending strike-slip shear zones, as expected in the case of displacements during a late phase of deformation. Rather, our data suggest strain partitioning along NE- and NW-trending segments, i.e., a general NNW-directed motion differentially accommodated in the form of frontal displacements in the NE-trending and shallower dipping segments, in association with oblique- to strike-slip motions along the NW steeply dipping segments, which possibly represent preexistent basement features. These local motions in fact reproduce the large-scale kinematic picture of the leading edge and eastern limb, which accommodate the NNW-directed motion along the segmented thrusts and the dextral Itapebi shear zone, respectively. A late phase reactivation of the NW-oriented structures cannot be ruled out. As noticed by Cruz and Alkmim (2006), the NNW-directed thrusts and associated folds are cut by a system of NNW-trending dextral strike-slip shear zones in the southern end of the adjacent Paramirim Corridor (these aspects are illustrated in Figs. 15, 16 and 17).

The existence of a  $D_1/D_2$  bivergent fold-thrust wedge in the interior of the hinge zone is another peculiar feature of

the Rio Pardo salient. As indicated by field observations and analogue modeling, double wedges develop in places where stresses of almost equal magnitudes and distributions act on opposite sides of a rock package (Marshak & Wilkerson 2004, Gomes *et al.* 2010, Forte *et al.* 2014). Our data, as shown on the cross-section of Figure 7, demonstrate that the double wedge of the Rio Pardo salient is quite asymmetric, with a relatively small retro-wedge and a large pro-wedge. In contrast to the previously mentioned analogue modeling, this asymmetry requires significant differences in the magnitude and distribution of stresses on opposite sides of the rock package, i.e. on the northern and southern sides of salient. Such a stress field could be generated by the underthrusting of the southern side of the basin beneath a buttress located on its northern side during the  $D_1/D_2$  phase. This buttress very likely corresponds to the basement high that defines the zigzag-shaped edge of the Macaúbas basin (Fig. 16).

The  $D_3$  phase corresponds to the last contractional episode documented in the region.  $D_3$  folds were observed only in the hinge zone (Fig. 7). The absence of these structures in the western limb can be explained in two ways. The ENE-WSW shortening responsible for their generation was accommodated only in the hinge zone or, alternatively, in different forms along the whole salient. In the latter case, the ENE-WSW shortening could be absorbed by a reactivation of the  $D_1/D_2$  structures in the western limb where they are NS-oriented, or even by an advance of deformation front further west, toward the craton interior. In fact, the collisional deformation, recorded by a system of thin-skinned folds and thrust, affected the Neoproterozoic cover of the

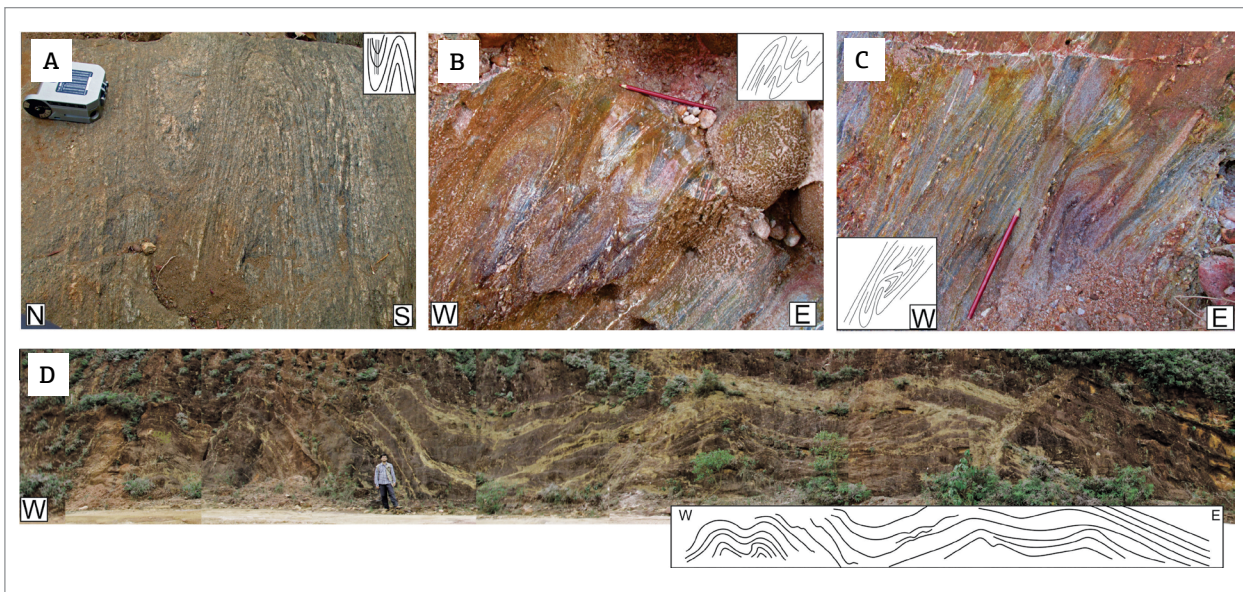


Figure 13. (A, B, C) Upright to slight inclined tight to isoclinal  $F_1$  folds, associated with subvertical  $S_1$  foliation in the eastern limb (A – plan view; B and C – cross-section view). (D) Open folds affecting  $S_1$  foliation, may be related to NS-oriented  $F_3$ -folds.

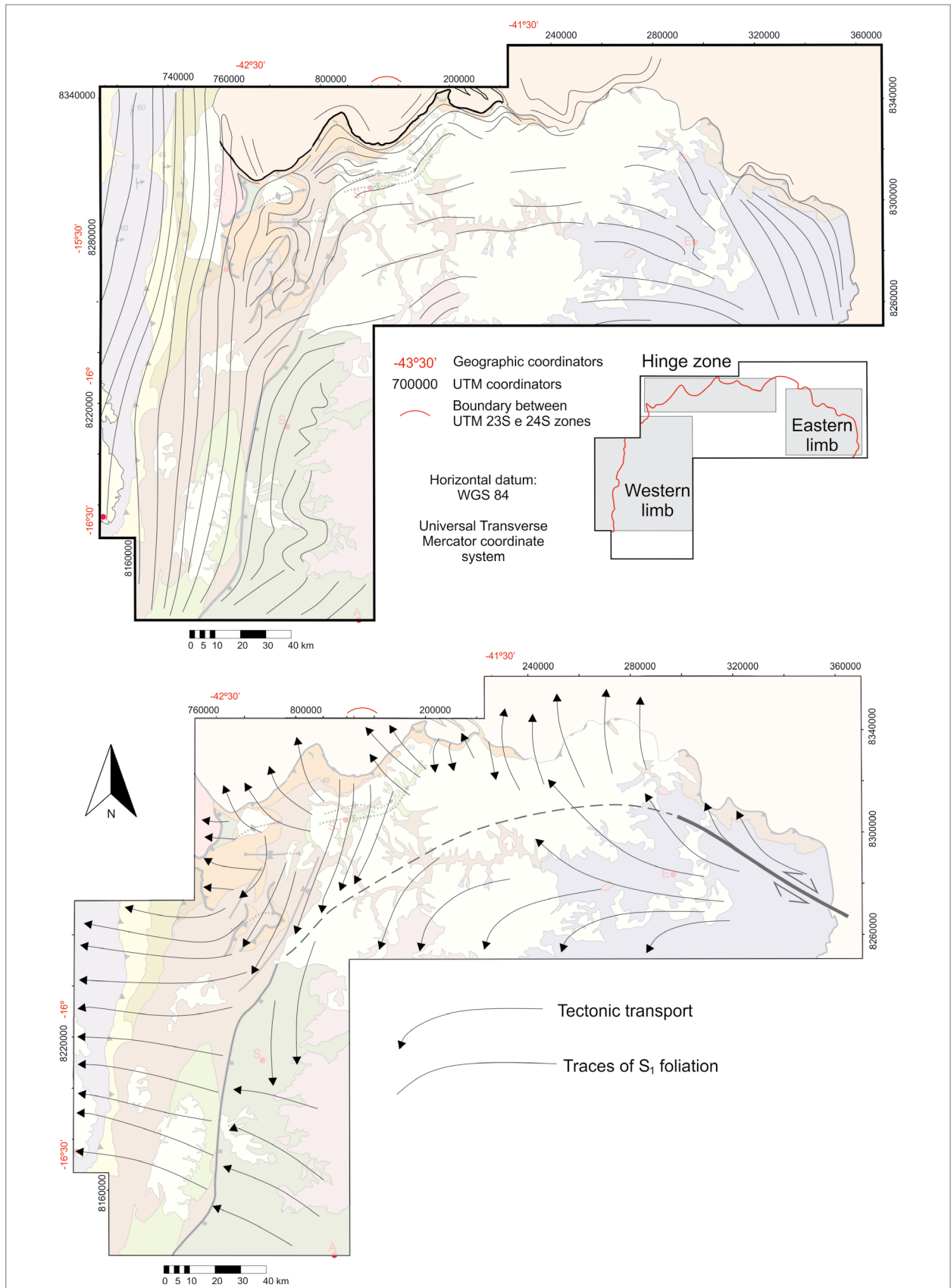


Figure 14. An integrated kinematic picture of the Rio Pardo salient, showing: (A) the traces of  $S_1$  foliation; (B) the tectonic transport, providing evidence for the vergence reversal of the hinge zone. The dashed line is an interpreted connection between the CASZ and the ISZ.

São Francisco craton over c. 50 km west of the leading edge of the western limb (Alkmim *et al.* 2017).

The extensional  $D_4$  deformation episode is recorded mainly by two regional normal-sense shear zones, the CASZ and the TSZ, as well as normal sinistral reactivation of the Itapepi shear zone. This phase, represented by a variety of structures in the Paramirim aulacogen (Cruz & Alkmim 2006, Cruz *et al.* 2007), is currently interpreted as the manifestation of the extensional collapse of the Araçuaí orogen (Marshak *et al.* 2006, Alkmim *et al.* 2006) (Figs. 5 and 17), recently dated at around 530 Ma in the western limb by Peixoto *et al.* (2018).

### Controlling factors of the salient generation

Salients can be generated either as primary arcs or oroclines (Marshak & Flöttmann 1996, Paulsen & Marshak 1999, Spraggins & Dunne 2002, Wilkerson *et al.* 2007, Williams *et al.* 2009, Gutiérrez-Alonso *et al.* 2012, Rosebaum *et al.* 2012, Chatzaras *et al.* 2013, Whisner *et al.* 2014, White *et al.* 2016, Szaniawski *et al.* 2017). The geological setting of the Rio Pardo salient makes its full development as an orocline impossible. In other words, its generation through the bending of an originally straight or considerably less-curved segment of the Araçuaí orogen would require a large rotation of the surrounding cratonic basement around a vertical axis, a mechanically unrealistic process. All features and processes discussed in the previous section strongly suggest that the Rio Pardo salient developed as a basin-controlled primary arc, which experienced a slight oroclinal enhancement during the  $D_3$  deformation phase. Its shape seems to reflect the original shape of the Macaúbas basin sector. Furthermore, as indicated by the distribution of the Macaúbas Group in the Araçuaí orogen, the salient is located in the main depocenter of the Macaúbas basin (Pedrosa-Soares *et al.* 2011a, Kuchenbecker *et al.* 2015), which was bounded on all sides by basement highs, represented by the Porteirinha block in the western limb, the Paramirim block in the culmination zone, and the large basement exposure adjacent to the eastern limb (Figs. 1 and 2). Another structural high must also exist farther south in the area presently occupied by the granite plutons of the crystalline core (Fig. 1) in order to have created the kinematic picture shown in Figure 14. In sum, the Rio Pardo salient can be simply viewed as a strongly inverted sector of the Macaúbas basin.

### Tectonic relationships with the Paramirim aulacogen

Fabric elements of the  $D_1$ ,  $D_3$  and  $D_4$  deformation episodes recognized in the salient have been previously documented in the southern Paramirim aulacogen (Cruz & Alkmim 2006, Cruz *et al.* 2007), where they characterize

the interaction zone between the Araçuaí orogenic front and the preexistent intracratonic rift structures (Cruz & Alkmim 2006). Fabric elements that could be ascribed to the  $D_2$  phase in the salient were not recognized in the aulacogen. Furthermore, the main accommodation form of the Brasiliano inversion in the aulacogen corresponds to two embryonic fold-thrust systems of opposite vergences. They are exposed along the northern Espinhaço ridge and western Chapada Diamantina, which together form the NNW-trending Paramirim deformation corridor, which was nucleated in response to a WSW-ENE-oriented shortening (Danderfer 2000, Cruz & Alkmim 2006, 2007, Bersan *et al.* 2017). In the salient, these structures could be represented by the elements of the  $D_3$  phase. However, the amount of shortening involved in the generation of these and the structures of the corridor are apparently incompatible. A possible solution for this problem seems to be, again, a significant strain partition between the distinct families of fabric elements occurring in both the corridor and the salient. In the next section, we present a model for the formation of the salient, which may account for this and other problems discussed above.

### An evolutionary model for the Rio Pardo salient

The data and interpretations presented here, along with worldwide studies on the origin and evolution of curve segments of f-t-belts, led us to propose the following model for the evolution of the Rio Pardo salient during the development of the Araçuaí-West Congo orogenic system, as portrayed by Alkmim *et al.* (2006).

- the Macaúbas basin stage (Fig. 15): the Macaúbas precursor basin probably started to open at around 900 Ma (Castro 2014, Pedrosa-Soares & Alkmim 2011, Kuchenbecker *et al.* 2015) and after renewed extensional pulses, eventually evolved into a large gulf connected to various intracontinental rift basins (the Pirapora, Paramirim, Nyanga, and Sangha aulacogens) and the Adamastor ocean (Fig. 15) at c. 680 Ma (Alkmim *et al.* 2006, 2007). The Macaúbas gulf separated the São Francisco peninsula from the Congo continent. Its northernmost (present-day coordinates) and ensialic portion was likely made up of a series of stepped basement grabens surrounded by basement highs, thereby delimiting a large and curved depocenter (Fig. 15);
- the Macaúbas basin closure and the salient formation stage (Fig. 16): the Macaúbas basin closure involved a progressive motion of the São Francisco peninsula against the Congo continent (Alkmim *et al.* 2006). During the convergence, east-direct subduction of the

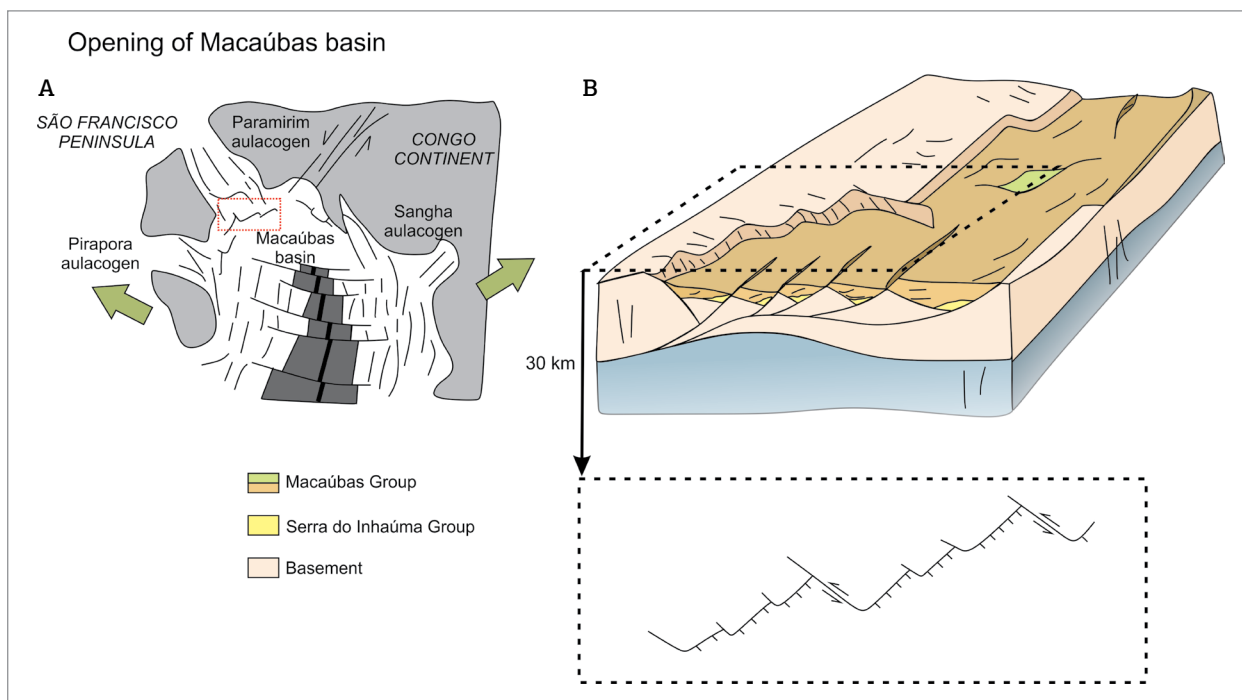


Figure 15. (A) An opening of the Macaúbas basin according to Alkmim *et al.* (2006). (B) Details of the basin geometry on the hinge zone, with stepped and steeply dipping segments in the north (current coordinates) and a shallow dipping basement in the inner portions of the orogen (southward).

Macaúbas basin oceanic floor led to the generation of the Rio Doce magmatic arc between 630 and 580 Ma (Pedrosa-Soares *et al.* 2001, 2008, Queiroga *et al.* 2007, Gonçalves *et al.* 2014, 2016). Once formed, the Rio Doce arc must have generated a large high to the south of the Macaúbas basin ensialic sector (Fig. 16A). With continued closure, the southern half of the depocenter rotated counterclockwise, pushing the Macaúbas rocks towards the western, northwestern and northern margins of the basin (i.e., the craton margins), and thus initiating the development of the salient (Fig. 16B). This process is recorded by the fabric elements of the  $D_1$  deformation phase, which started to define the complex motion picture of the salient, largely influenced by the pre-orogenic basement structures of the basin. These initial motions must have been accommodated by relatively small inversion strains in the aulacogens connected to the gulf, especially in the Paramirim. As convergence progressed, the Paramirim aulacogen underwent major inversion. Whilst in the salient, the deformations were accommodated by the  $D_2$  structures (Fig. 16B). Full development of the Paramirim corridor as a consequence of the final closure of the Macaúbas basin was recorded in the salient by the  $D_3$  deformation phase, which led to the reactivation of preexistent structures and the enhancement of the salient curvature (Fig. 16C). The overall geometry of the resulting curvature may be seen as a consequence

of three main control factors, as illustrated in Figures 16D, 16E and 16F:

- the presence of stepped basement blocks along the cratonic margins;
- the deformation partitioning of the overall NW tectonic transport along NE- and NW-trending basement segments, i.e. a compressional deformation system along NE-trending boundaries and a transpressional system along NW-trending segments;
- the enhancement of the curvature during  $D_3$  phase, which gives rise to an regional WSW-ENE shortening. Also, the change of vergence, as illustrated by the VD-line (Fig. 7), is attributed to the position of the supracrustal rocks in relation to the basement.

Folds and thrusts show top-up-to-the-south vergence close to NW-trending segments, while in NE-trending segments this vergence is observed only around 10km away from the contact with the basement-supracrustal rocks (Figs. 16E and 16F). The final closure of the Macaúbas basin is currently connected to the collisional stage of the AWCO, which took place in the interval of 575–565 Ma (Pedrosa-Soares *et al.* 2001, 2011a, Silva *et al.* 2011, Melo *et al.* 2017a, 2017b, Peixoto *et al.* 2015, 2018, Richter *et al.* 2016).

- The extensional collapse stage (Fig. 17): the thickened internal portion of the Rio Pardo salient was affected

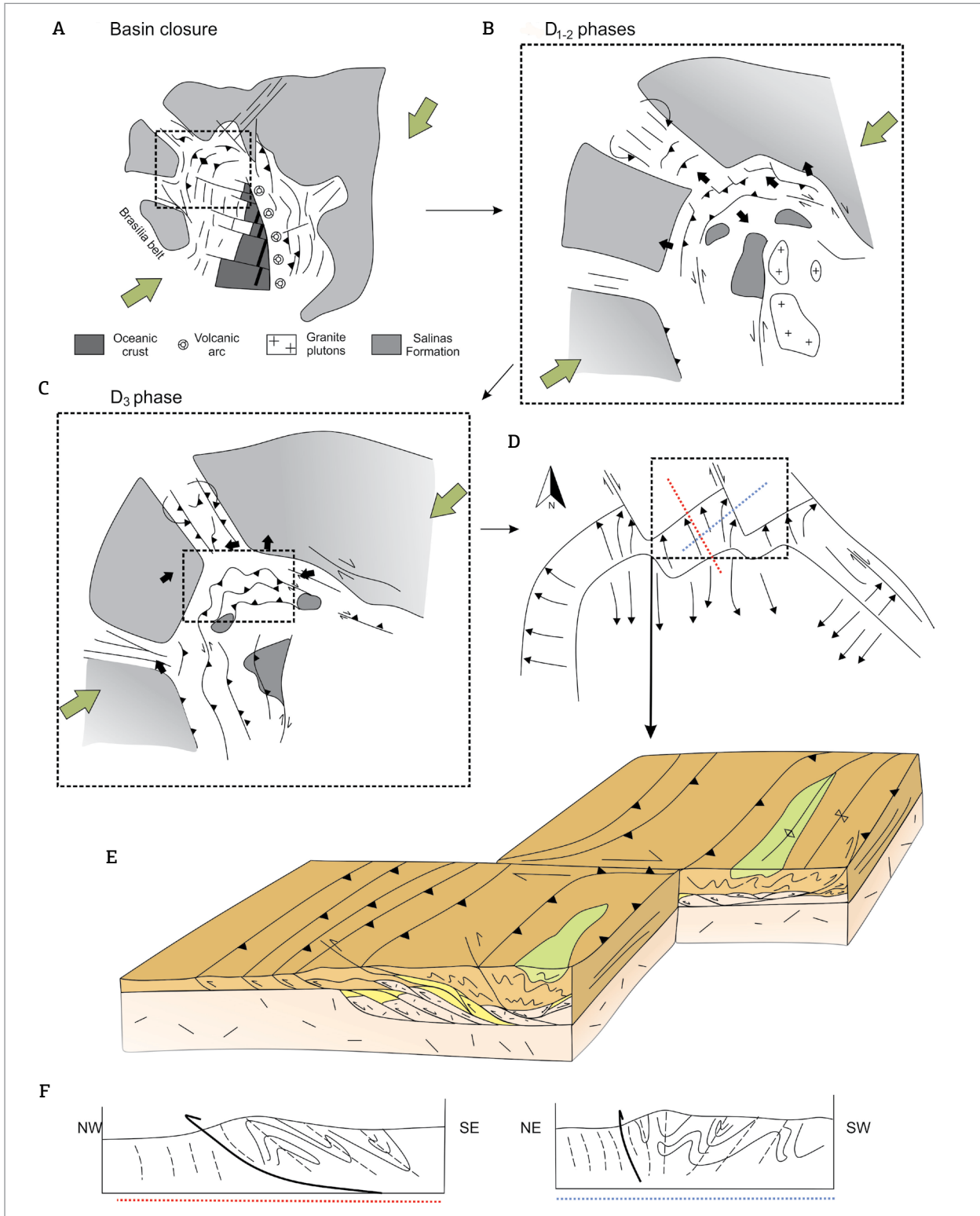


Figure 16. (A) The closure of the Macaúbas basin and the formation of the magmatic arc (Alkmim *et al.* 2006). The Macaúbas basin in the ensialic sector is confined to basement horsts in the north and to the magmatic arc in the south. (B) Details of the main phases of the collisional stage (D<sub>1-2</sub>), with supracrustal rocks deformed under a vergence reversal system. Deposition of the syn-collisional Salinas Formation along the orogen. (C) Final shortening and D<sub>3</sub> structures development, with structural trends similar to the Paramirim corridor. (D, E) Details of the strain partitioning along the leading edge, represented by thrust zones along NE-trending segments and reversal-dextral shear zones along NW-trending segments. (F) Schematic cross-sections of each segment, with the vergence reversal occurring nearer to basement-supracrustal contact along NW-trending segments than to NE-trending segments.

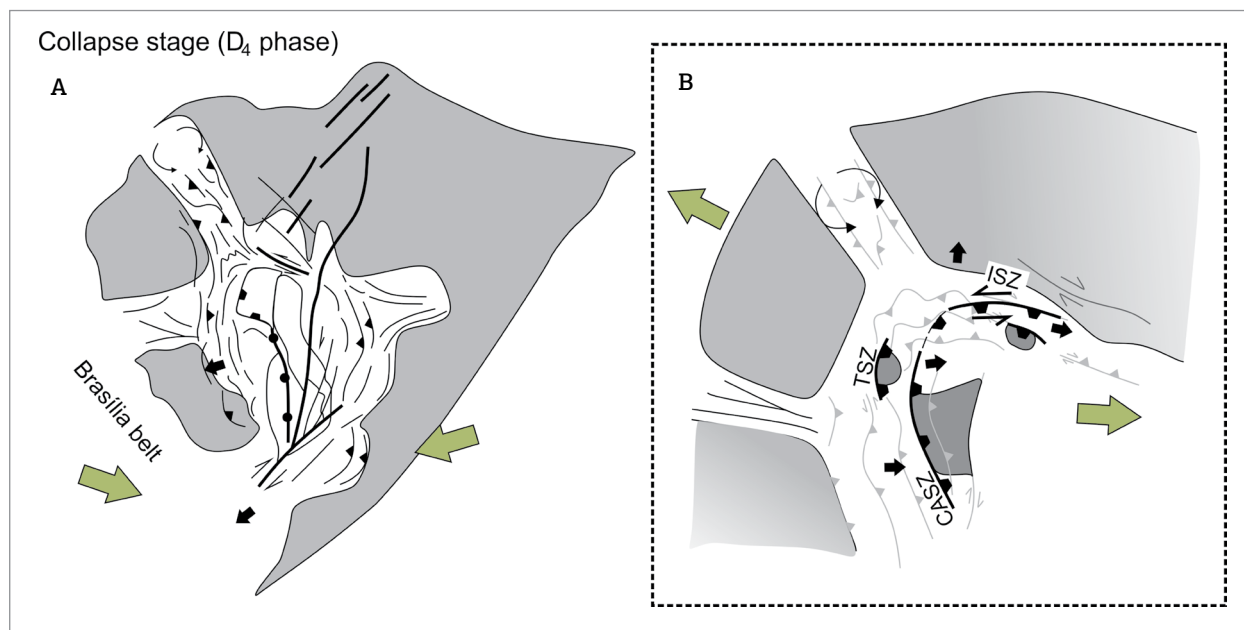


Figure 17. The collapse stage of the Araçuaí orogen (Alkmim *et al.* 2006) and the development of the CASZ, the TSZ and the normal-sinistral reactivation of the ISZ. Upper crustal level units (e.g. the Salinas Formation) are brought to lower crustal level, as they are located on the hanging wall of these normal-sense shear zones.

by extensional tectonism at c. 530 Ma (Alkmim *et al.* 2006, Marshak *et al.* 2006, Peixoto *et al.* 2018), and was recorded mainly by  $D_4$  large-scale Chapada Acauã and Tingui normal-sense shear zones. Starting at this time, a large number of post-collisional plutons intruded the Macaúbas Group in the central portion of the salient.

## CONCLUSIONS

Our structural study on the Rio Pardo salient led to the following conclusions:

- the salient formed in response to four deformational phases. The contractional  $D_1$  and  $D_2$  phases record a craton-directed tectonic transport in the outer arc, coupled with an overall southward motion in the inner arc, thereby characterizing a double fold-thrust wedge. Along the salient's leading edge, structures of  $D_1/D_2$  phases define a zigzag pattern with alternating NE- and NW-trending segments. Along the NE-trending segments, the metasedimentary rocks are thrust northwards on top of the basement, while along the NW-trending segments, they are juxtaposed with the basement through reverse-dextral shear zones. The  $D_3$  phase, which is recorded only in the hinge zone, led to the nucleation of NNW-trending folds, and caused an enhancement of the salient under an approximately WSW-ENE contractional stress field.

The fourth  $D_4$  phase is recorded mainly by a set of extensional structures;

- the contractional  $D_1$ ,  $D_2$  and  $D_3$  deformation phases represent the collisional stage of the development of Araçuaí-West Congo orogen, dated between 575 and 565 Ma. The  $D_4$  extensional phase, dated at c. 530 Ma, can be correlated to the extensional collapse of the orogen;
- the overall architecture and the kinematic picture we describe suggest that the Rio Pardo salient was generated as a primary arc, and was strongly controlled by the shape of the Macaúbas basin. The double fold-thrust wedge formed during the  $D_1$ - $D_2$  phases seems to result from the closure of a curved depocenter, bounded to the north and south sides by basement highs. During the  $D_3$  WSW-ENE shortening, the curvature of the salient was enhanced;
- the salient evolution characterizes a case of strain partitioning during the closure of the Macaúbas basin and the generation of the Araçuaí-West Congo orogen.

## ACKNOWLEDGMENTS

The authors acknowledge the financial support provided by the following Brazilian research and development agencies: CAPES (to E. Peixoto) and CNPq (grant # 308045/2013-0, to F.Alkmim).

## REFERENCES

- Alkmim F.F., Kuchenbecker M., Reis H.L.S., Pedrosa-Soares A.C. 2017. *The Araçuaí Belt. Regional Geology Reviews*. Switzerland, Springer International Publishing. p. 255-276.
- Alkmim F.F., Marshak S., Pedrosa-Soares A.C., Peres G.G., Cruz S.C.P., Whittington A. 2006. Kinematic Evolution of the Araçuaí–West Congo orogen in Brazil and Africa: Nutcracker tectonics during the Neoproterozoic assembly of Gondwana. *Precambrian Research*, **149**:43-64. <https://doi.org/10.1016/j.precamres.2006.06.007>
- Alkmim F.F., Pedrosa-Soares A.C., Noce C.M., Cruz S.C.P. 2007. Sobre a evolução tectônica do Orógeno Araçuaí-Congo Ocidental. *Geonomos*, **15**(1):25-43. <http://dx.doi.org/10.18285/geonomos.v15i1.105>
- Almeida F.F.M. 1977. O Cráton do São Francisco. *Revista Brasileira de Geociências*, **7**:349-364.
- Almeida F.F.M., Hassui Y., Rodrigues E.P., Yakamoto J.K. 1978. A Faixa de dobramentos Araçuaí na região do Rio Pardo. In: Congresso Brasileiro de Geologia, 30, Recife. *Anais...*, **1**:270-283.
- Babinski M., Pedrosa-Soares A.C., Trindade R.I.F., Martins M., Noce C.M., Liu D. 2012. Neoproterozoic glacial deposits from the Araçuaí orogen, Brazil: Age, provenance and correlations with the São Francisco craton and West Congo belt. *Gondwana Research*, **21**:451-465. <http://dx.doi.org/10.1016/j.gr.2011.04.008>
- Barbosa J.S.F., Correa-Gomes L.C., Marinho M.M., Silva F.C.A. 2003. Geologia do segmento sul do Orógeno Itabuna-Salvador-Curaçá. *Revista Brasileira de Geociências*, **33**:33-47.
- Barbosa J.S.F., Cruz S.C.P., Souza J.S. 2012. Terrenos metamórficos do embasamento. In: Barbosa, J.S.F. (coord.), *Geologia da Bahia: pesquisa e atualização*. Salvador: Convênio CBPM-UFBA, p. 101-201.
- Barbosa J.S.F. & Dominguez J.M.L. 1996. *Mapa Geológico do Estado da Bahia*. Escala 1:1.00.000. Texto Explicativo, Salvador, 382 p.
- Bersan S.M., Danderfer A., Lagoeiro L., Costa A.F.O. 2017. The kinematic evolution of the Serra Central Salient, Eastern Brazil: a Neoproterozoic progressive arc in northern Espinhaço fold-thrust belt. *Journal of South American Earth Sciences*, **80**:131-148. <https://doi.org/10.1016/j.jsames.2017.09.013>
- Beutner E.C. 1977. Causes and consequences of curvature in the Sevier orogenic belt, Utah to Montana, in Rocky Mountain thrust belt, geology and resources: Wyoming. *Geological Association Annual Field Conference Guidebook*, **29**:353-365.
- Boyer S.E. 1995. Sedimentary basin taper as a factor controlling the geometry and advance of thrust belts. *American Journal of Science*, **295**:1220-1254. DOI: 10.2475/ajs.295.10.1220
- Castro M.P. 2014. *Caracterização geológica da Formação Capelinha como uma unidade basal do Grupo Macaúbas em sua área tipo, Minas Gerais*. Dissertation, Departamento de Geologia, Universidade Federal de Ouro Preto, Ouro Preto.
- Chatzaras V., Xypolias P., Kokkalas S., Koukouvelas I. 2013. Tectonic evolution of a crustal-scale oblique ramp, Hellenides thrust belt, Greece. *Journal of Structural Geology*, **57**:16-37. <https://doi.org/10.1016/j.jsg.2013.10.003>
- Chemale Jr. F., Dussin I.A., Alkmim F.F., Martins M.S., Queiroga G., Armstrong R., Santos M.N. 2012. Unravelling a Proterozoic basin history through detrital zircon geochronology: The case of the Espinhaço Supergroup, Minas Gerais, Brazil. *Gondwana Research*, **22**:200-206. <https://doi.org/10.1016/j.gr.2011.08.016>
- Cordani U. 1973. *Evolução geológica pré-cambriana da faixa costeira do Brasil, entre Salvador e Vitória*. Thesis, Instituto de Geociências, Universidade de São Paulo, São Paulo, 312 p.
- Corrêa-Gomes L.C. 2000. *Evolução dinâmica da zona de cisalhamento neoproterozoica de Itabuna-Itaju do Colônia e do magmatismo fissural alcalino associado (SSE da Bahia, Brasil)*. Thesis, Instituto de Geociências, Universidade Estadual de Campinas, Campinas, 362 p.
- Costa A.F. & Danderfer F.A. 2017. Tectonics and sedimentation of the central sector of the Santo Onofre rift, north Minas Gerais, Brazil. *Brazilian Journal of Geology*, **47**(3):491-519. <http://dx.doi.org/10.1590/2317-4889201720160128>
- Cruz S., Alkmim F., Pedreira A.J., Teixeira L.R., Pedrosa-Soares A.C., Corrêa-Gomes L.C., Souza J.S., Leal A.B.M. 2012a. Orógeno Araçuaí. In: Barbosa, J.S.F. (coord.), *Geologia da Bahia: pesquisa e atualização*. Salvador: Convênio CBPM-UFBA, p. 31-177.
- Cruz S.C.P., Dias V.M. & Alkmim F.F. 2007. A interação tectônica embasamento/cobertura em aulacógenos invertidos: um exemplo da Chapada Diamantina Ocidental. *Revista Brasileira de Geociências*, **37**(4):111-127.
- Cruz S.C.P. & Alkmim F.F. 2006. The tectonic interaction between the Paramirim aulacogen and the Araçuaí belt, São Francisco craton region, Eastern Brazil. *Anais da Academia Brasileira de Ciências*, **78**(1):151-173. <http://dx.doi.org/10.1590/S0001-37652006000100014>
- Cruz S.C.P. & Alkmim F. 2007. A história de inversão do aulacógeno do Paramirim contada pela sinclinal de Ituaçu, extremo sul da Chapada Diamantina (BA). *Revista Brasileira de Geociências*, **37**(4):92-110.
- Cruz S.C.P., Peucat J.J., Teixeira L., Carneiro M.A., Martins A.A.M., Santana J.S., Souza J.S., Barbosa J.S.F., Leal A.B.M., Dantas E., Pimentel, M. 2012b. The Caraguataí syenitic suite, a ca. 2.7 Ga-old alkaline magmatism (petrology, geochemistry and U-Pb zircon ages). Southern Gavião block (São Francisco Craton), Brazil. *Journal of South American Earth Sciences*, **37**:95-112. DOI: 10.1016/j.jsames.2011.11.006
- Danderfer A. 2000. *Geologia Sedimentar e Evolução Tectônica do Espinhaço Setentrional*. Thesis, Universidade de Brasília, Brasília, 498 p.
- Danderfer A. & Dardenne M.A. 2002. Tectonoestratigrafia da bacia Espinhaço na porção centro—norte do cráton do São Francisco: registro de uma evolução polistórica descontínua. *Revista Brasileira de Geociências*, **32**(4):449-460.
- Danderfer F.A., DeWaele B., Pedreira A.J., Nalini H.A. 2009. New geochronological constraints on the geological evolution of Espinhaço basin within the São Francisco Craton—Brazil. *Precambrian Research*, **170**:116-128. <https://doi.org/10.1016/j.precamres.2009.01.002>
- Davis D., Suppe J., Dahlen F. 1983. Mechanics of fold-and-thrust belts and accretionary wedges. *Journal of Geophysical Research*, **88**:1153-1172. DOI: 10.1029/JB088iB02p01153
- De Campos C.M. de, Mendes J.C., Ludka I.P., Medeiros S.R., Moura J.C. & Wallfuss C. 2004. A review of the Brasiliano magmatism in southern Espírito Santo, Brazil, with emphasis on postcollisional magmatism. *Journal of the Virtual Explorer*, **17**. DOI: 10.3809/jvirtex.2004.00106
- De Campos C.P., Medeiros S.R., Mendes J.C., Pedrosa-Soares A.C., Dussin I., Ludka I.P., Dantas E.L. 2016. Cambro-Ordovician magmatism in the Araçuaí Belt (SE Brazil): Snapshots from a post-collisional event. *Journal of South American Earth Sciences*, **68**:248-268. <https://doi.org/10.1016/j.jsames.2015.11.016>

- Dussin I.A. & Dussin T.M. 1995. Supergrupo Espinhaço: Modelo de Evolução e Geodinâmica. *Geonomos*, **3**(1):19-26. <http://dx.doi.org/10.18285/geonomos.v3i1.212>
- Eldredge S., Bachtadse V., Van der Voo R. 1985. Paleomagnetism and the orocline hypothesis. *Tectonophysics*, **119**:153-179. [https://doi.org/10.1016/0040-1951\(85\)90037-X](https://doi.org/10.1016/0040-1951(85)90037-X)
- Forte A.M., Cowgill E.S., Whipple K.X. 2014. Transition from a singly to doubly-vergent wedge in a young orogen: The Greater Caucasus. *Tectonics*, **33**:2077-2101. DOI: 10.1002/2014TC003651
- Gomes C.J.S., Danderfer Filho A., Posada A.M., da Silva A. 2010. The role of backstop shape during inversion tectonics physical models. *Anais da Academia Brasileira de Ciências*, **82**(4):997-1012. <http://dx.doi.org/10.1590/S0001-37652010000400021>
- Gonçalves-Dias T., Caxito F.A., Pedrosa-Soares A.C., Stevenson R., Dussin I., Silva L.C., Alkmim F., Pimentel M. 2016. Age, provenance and tectonic setting of the high-grade Jequitinhonha Complex, Araçuaí Orogen, eastern Brazil. *Brazilian Journal of Geology*, **46**(2):199-219. <http://dx.doi.org/10.1590/2317-4889201620160012>
- Gonçalves-Dias T., Pedrosa-Soares A.C., Dussin I.A., Alkmim F.F., Caxito F.A., Silva L.C., Noce C.M. 2011. Maximum sedimentation age and provenance of the Jequitinhonha Complex in the type-area (Araçuaí orogen): First U-Pb (LA-ICP-MS) data from detrital zircon grains. *Geonomos*, **19**:121-130.
- Gonçalves L., Alkmim F., Pedrosa-Soares A.C., Dussin I.A., Valeriano C.M., Lana C., Tedeschi M. 2016. Granites of the Intracontinental Termination of a Magmatic Arc: an Example from the Ediacaran Araçuaí Orogen, Southeastern Brazil. *Gondwana Research*, **36**:439-458. <https://doi.org/10.1016/j.gr.2015.07.015>
- Gonçalves L., Farina F., Lana C., Pedrosa-Soares A.C., Alkmim F., Nalini Jr. H.A. 2014. New U-Pb ages and lithochemical attributes of the Ediacaran Rio Doce magmatic arc, Araçuaí confined orogen, southeastern Brazil. *Journal of South American Earth Sciences*, **52**:129-148. <https://doi.org/10.1016/j.jsames.2014.02.008>
- Gradim C., Roncato J., Pedrosa-Soares A.C., Cordani U., Dussin I., Alkmim F.F., Queiroga G., Jacobsohn T., Silva L.C., Babinski M. 2014. The hot back-arc zone of the Araçuaí orogen, Eastern Brazil: from sedimentation to granite generation. *Brazilian Journal of Geology*, **44**(1):155-180. DOI: 10.5327/Z2317-4889201400010012
- Grossi-Sad J.H., Lobato L.M., Pedrosa-Soares A.C., Soares-Filho B.S. 1997. *Projeto Espinhaço em CD-ROM (textos, mapas e anexos)*. Belo Horizonte, Companhia Mineradora de Minas Gerais.
- Gutiérrez-Alonso G., Fernández-Suárez J., Weil A.B. 2004. Orocline triggered lithospheric delamination. *Special Papers - Geological Society of America*, **383**:121-131. [https://doi.org/10.1130/0-8137-2383-3\(2004\)383\[121:OTLD\]2.0.CO;2](https://doi.org/10.1130/0-8137-2383-3(2004)383[121:OTLD]2.0.CO;2)
- Gutiérrez-Alonso G., Johnson S.T., Weil A.B., Pastor-Galán D., Fernández-Suárez J. 2012. Buckling an orogen: the Cantabrian Orocline. *GSA Today*, **22**(7):4-9. DOI: 10.1130/GSATG141A.1
- Inda H.A.V. & Barbosa J.F. 1978. *Texto explicativo para mapa geológico do Estado da Bahia: escala 1:1.000.000*. Salvador: SME, COM.
- Knauer L.G., Pereira D.F.L.C., Guimarães F.S., Fantinel L.M., Costa R.D. 2015. Geologia da folha Mortugaba. In: Pedrosa-Soares A.C. (coord.). *Projeto Fronteiras de Minas*. Belo Horizonte, CODEMIG-UFMG.
- Kuchenbecker M., Pedrosa-Soares A.C., Babinski M., Fanning M. 2015. Detrital zircon age patterns and provenance assessment for pre-glacial to post-glacial successions of the Neoproterozoic Macaúbas Group, Araçuaí orogen, Brazil. *Precambrian Research*, **266**:12-26. <https://doi.org/10.1016/j.precamres.2015.04.016>
- Laubscher H.P. 1972. Some overall aspects of the Jura dynamics. *American Journal of Science*, **272**:293-304. DOI: 10.2475/ajs.272.4.293
- Lima M.I.C., Fonseca E.G. da, Oliveira E.P., Ghignone J.I., Rocha R.M., Carmo V.F., Silva J.M.R., Siga Jr. O. 1981. Folha SD. 24 Salvador; geologia, geomorfologia, pedologia, vegetação e uso potencial da terra. *Projeto RADAMBRASIL*. Rio de Janeiro, p. 25-192.
- Lima S.A.A., Martins-Neto M., Pedrosa-Soares A.C., Cordani U.G., Nutman A. 2002. A Formação Salinas na área tipo, NE de Minas Gerais: uma proposta de revisão da estratigrafia da Faixa Araçuaí com base em evidências sedimentares, metamórficas, e idades U-Pb SHRIMP. *Revista Brasileira de Geociências*, **32**:491-500.
- Macedo J.M. & Marshak S. 1999. Controls on the geometry of fold-thrust belt salients. *Geological Society of America Bulletin*, **111**:1808-1822. [https://doi.org/10.1130/0016-7606\(1999\)111%3C1808:COTGOF%3E2.3.CO;2](https://doi.org/10.1130/0016-7606(1999)111%3C1808:COTGOF%3E2.3.CO;2)
- Machado N., Schrank A., Abreu F.R., Knauer L.G., Almeida-Abreu P.A. 1989. Resultados preliminares da geocronologia U-Pb na Serra do Espinhaço Meridional. *Boletim do Núcleo Minas Gerais-Sociedade Brasileira de Geologia*, **10**:171-174.
- Marinho M.M., Sabaté P., Barbosa J.S.F. 1994. The Contendas-Mirante volcano-sedimentary belt. *Boletim IG-USP*, **17**:37-72.
- Marshak S. 2004. Salients, recesses, arcs, oroclines and syntaxes – A review of ideias concerning the formation of map-view curves in fold-thrust belts. In: MacClay K.R. (ed.), *Thrust tectonics and hydrocarbon systems*. AAPG Memoir, **82**:131-156.
- Marshak S., Alkmim F.F., Whittington A. & Pedrosa-Soares A.C. 2006. Extensional collapse in the Neoproterozoic Araçuaí orogen, eastern Brazil: A setting for reactivation of asymmetric crenulation cleavage. *Journal Structural Geology*, **28**:129-147.
- Marshak S. & Flöttmann T. 1996. Structure and origin of the Fleurieu and Nackara arcs in the Adelaide foldthrust belt, South Australia; salient and recess development in the Delamerian orogen. *Journal of Structural Geology*, **18**:891-908. [https://doi.org/10.1016/0191-8141\(96\)00016-8](https://doi.org/10.1016/0191-8141(96)00016-8)
- Marshak S. & Wilkerson M.S. 1992. Effect of overburden thickness on thrust-belt geometry and development. *Tectonics*, **11**:560-566. DOI: 10.1029/92TC00175
- Marshak S. & Wilkerson M.S. 2004. Fold-thrust belts. In: Van der Pluijm B.A. & Marshak, S. (eds.), *Earth Structure*. 2ª ed. New York: W. W. Norton & Co., New York, p. 444-474.
- Martins-Neto M.A. 2000. Tectonics and Sedimentation In A Proterozoic Rift-Sag Basin (Espinhaço Basin, Southeastern Brazil). *Precambrian Research*, **103**:147-173.
- Melo M.G., Lana C., Stevens G., Pedrosa-Soares A.C., Gerdes A., Alkmim L.A., Nalini Jr H.A., Alkmim F.F. 2017a. Assessing the isotopic evolution of S-type granites of the Carlos Chagas Batholith, SE Brazil: Clues from U-Pb, Hf isotopes, Ti geothermometry and trace element composition of zircon. *Lithos*, **284-285**:730-750. <https://doi.org/10.1016/j.lithos.2017.05.025>
- Melo M.G., Stevens G., Lana C., Pedrosa-Soares A.C., Frei D., Alkmim F.F., Alkmim L.A. 2017b. Two cryptic anatexis events within a syn-collisional granitoid from the Araçuaí orogen (southeastern Brazil): Evidence from the polymetamorphic Carlos Chagas batholith. *Lithos*, **277**:51-71. <https://doi.org/10.1016/j.lithos.2016.10.012>
- Moraes Filho J.C.R. & Lima E.S. 2007. *Região de Itapetinga, sul da Bahia (borda SE do Cráton do São Francisco): geologia e recursos minerais*. Salvador, CBPM, CPRM, 2007. Inclui 1 mapa colorido. (Série Arquivos Abertos, 27).
- Noce C.M., Pedrosa-Soares A.C., Grossi-Sad J.H., Baars F.J., Guimarães M.L.V., Mourão M.A.A., Oliveira M.J.R., Roque N.C. 1997. Nova divisão estratigráfica regional do Grupo Macaúbas na Faixa Araçuaí: O registro de uma bacia neoproterozóica. In: Simpósio de Geologia de Minas Gerais, 9, 1997, Ouro Preto. *Anais...*, **14**:29-31.

- Noce C.M., Pedrosa-Soares A.C., Silva L.C., Alkmim F.F. 2007a. O Embasamento Arqueano e Paleoproterozóico do Orógeno Araçuaí. *Geonomos*, **15**:17-23. <http://dx.doi.org/10.18285/geonomos.v15i1.104>
- Noce C.M., Pedrosa-Soares A.C., Silva L.C., Armstrong R. & Piuçana D. 2007b. Evolution of polycyclic basement complexes in the Araçuaí orogen, based on U-Pb SHRIMP data: Implications for Brazil–Africa links in Paleoproterozoic time. *Precambrian Research*, **159**:60-78. <https://doi.org/10.1016/j.precamres.2007.06.001>
- Paes V.J.C., Raposo F.O., Pinto C.P., Oliveira F.A.R. 2010. *Projeto Jequitinhonha, Estados de Minas Gerais e Bahia: texto explicativo*. Geologia e Recursos Minerais das Folhas Comercinho, Jequitinhonha, Almenara, Itaobim, Joaíma e Rio do Prado. Programa Geologia do Brasil. Belo Horizonte, CPRM, 376 p.
- Paixão M.M. & Perrella P. 2004. *Mapeamento geológico da área do contato entre o Maciço Granítico Salto da Divisa e o Complexo Jequitinhonha, nordeste de Minas Gerais*. Graduation course, Departamento de Geologia, Universidade Federal de Minas Gerais, Belo Horizonte, 196 p.
- Pastor-Galán D., Gutierrez-Alonso G., Weil A.B. 2011. Orocline timing through joint analysis: insights from the Ibero-Armorican Arc. *Tectonophysics*, **507**:31-46. <https://doi.org/10.1016/j.tecto.2011.05.005>
- Paulsen T. & Marshak S. 1999. Origin of the Uinta recess, Sevier fold-thrust belt, Utah: Influence of basin architecture on fold-thrust belt geometry. *Tectonophysics*, **312**:203-216. [http://dx.doi.org/10.1016/S0040-1951\(99\)00182-1](http://dx.doi.org/10.1016/S0040-1951(99)00182-1)
- Pedrosa-Soares A.C. & Alkmim F.F. 2011. How many rifting events preceded the development of the Araçuaí–West Congo orogen? *Geonomos*, **19**(2):244-251. <http://dx.doi.org/10.18285/geonomos.v19i2.56>
- Pedrosa-Soares A.C. & Wiedmann-Leonardos C.M. 2000. Evolution of the Araçuaí Belt and its connection to the Ribeira Belt, Eastern Brazil. In: Cordani U., Milani E., Thomaz-Filho A., Campos, D.A. (eds.), *Tectonic Evolution of South America*. 31st International Geological Congress, Rio de Janeiro, p. 265-285.
- Pedrosa-Soares A.C., Alkmim F.F., Tack L., Noce C.M., Babinski M., Silva L.C., Martins-Neto M. 2008. Similarities and differences between the Brazilian and African counterparts of the Neoproterozoic Araçuaí–West Congo Orogen. In: Pankhurst J.R., Trouw R.A.J., Brito Neves B.B., De Wit M.J. (eds.), *West Gondwana: Pre-Cenozoic Correlations across the South Atlantic Region*. *Geological Society, London, Special Publications*, **294**:153-172.
- Pedrosa-Soares A.C., Babinski M., Noce C., Martins M., Queiroga G., Vilela F. 2011a. The Neoproterozoic Macaúbas Group (Araçuaí orogen, SE Brazil) with emphasis on the diamictite formations. In: Araud E., Halverson G.P. & Shields-Zhou G. (eds.), *The Geological Record of Neoproterozoic Glaciations*. *Geological Society, London, Memoirs*, **36**:523-534.
- Pedrosa-Soares A.C., De Campo C.P., Noce C., Silva L.C., Novo T., Roncato R., Medeiros S., Castañeda C., Queiroga G., Dantas E., Dussin I., Alkmim F. 2011b. Late Neoproterozoic–Cambrian granitic magmatism in the Araçuaí orogen (Brazil), the Eastern Brazilian Pegmatite Province and related mineral resources. *Geological Society, London, Special Publications*, **350**:25-51. <https://doi.org/10.1144/SP350.3>
- Pedrosa-Soares A.C., Noce C.M., Alkmim F.F., Silva L.C., Babinski M., Cordani U., Castañeda C. 2007. Orógeno Araçuaí: síntese do conhecimento 30 anos após Almeida 1977. *Geonomos*, **15**:1-16.
- Pedrosa-Soares A.C., Noce C.M., Wiedemann C.M., Pinto C.P. 2001. The Araçuaí–West Congo Orogen in Brazil: An overview of a confined orogen formed during Gondwanaland assembly. *Precambrian Research*, **110**:307-323. [https://doi.org/10.1016/S0301-9268\(01\)00174-7](https://doi.org/10.1016/S0301-9268(01)00174-7)
- Pedrosa-Soares A.C., Vidal P., Leonardos O.H., Brito-Neves B.B. 1998. Neoproterozoic oceanic remnants in eastern Brazil: further evidence and refutation of an exclusively ensialic evolution for the Araçuaí–West Congo Orogen. *Geology*, **26**:519-522. [https://doi.org/10.1130/0091-7613\(1998\)026%3C0519:NORIEB%3E2.3.CO;2](https://doi.org/10.1130/0091-7613(1998)026%3C0519:NORIEB%3E2.3.CO;2)
- Peixoto E., Alkmim F.F., Pedrosa-Soares A., Lana C., Chaves A.O. 2018. Metamorphic record of collision and collapse in the Ediacaran–Cambrian Araçuaí orogen, SE-Brazil: Insights from P-T pseudosections and monazite dating. *Journal of Metamorphic Geology*, **36**(2):147-172. DOI: 10.1111/jmg.12287.
- Peixoto E., Pedrosa-Soares A.C., Alkmim F.F., Dussin I.A. 2015. A suture-related accretionary wedge formed in the Neoproterozoic Araçuaí orogen (SE Brazil) during Western Gondwanaland assembly. *Gondwana Research*, **27**:878-896. <https://doi.org/10.1016/j.gr.2013.11.010>
- Peixoto E.I.N. 2017. *Arquitetura e evolução tectono-metamórfica da Saliência do Rio Pardo, Orógeno Araçuaí, MG*. Thesis, Departamento de Geologia, Escola de Minas, Universidade Federal de Ouro Preto, Ouro Preto.
- Peres G.G., Alkmim F.F., Jordt-Evangelista H. 2004. The southern Araçuaí belt and the DomSilvério Group: Geologic architecture and tectonic significance. *Anais Academia Brasileira de Ciências*, **76**:771-790. <http://dx.doi.org/10.1590/S0001-37652004000400011>
- Pinto C.P., Drumond J.B.V., Féboli W.L. 2001. *Projeto Leste, Etapas 1 e 2*. Belo Horizonte, CPRM-COMIG. 1 CD-ROM.
- Portela H.C.P., Machetto C.M.L., Santos E.L., Meneguesso G., Stein J.H., Moutinho da Costa L.A., Batista M.B., Messmann R., Silva W.G. 1976. *Projeto Leste do Tocantins/Oeste do Rio São Francisco*. Relatório Final, Fase V, Texto, volume 1a, 300 p.
- Prasad B.R., Klemperer S.L., Rao V.V., Tewari H.C., Khare P. 2011. Crustal structure beneath the Sub-Himalayan fold-thrust belt, Kangra recess, northwest India, from seismic reflection profiling: implications for Late Paleoproterozoic orogenesis and modern earthquake hazard. *Earth Planetary Science Letters*, **308**:218-228. DOI: 10.1016/j.epsl.2011.05.052
- Queiroga G., Pedrosa-Soares A.C., Noce C.M., Alkmim F.F., Pimentel M.M., Dantas E., Martins M., Castañeda C., Saita M.T.F., Prichard F. 2007. Age of the Ribeirão da Folha ophiolite, Araçuaí Orogen: The U-Pb zircon dating of a plagiogranite. *Geonomos*, **15**:61-65.
- Reis H.L.S., Alkmim F.F. 2015. Anatomy of a basin-controlled foreland fold-thrust belt curve: The Três Marias salient, São Francisco basin, Brazil. *Marine and Petroleum Geology*, **66**:711-731. <https://doi.org/10.1016/j.marpetgeo.2015.07.013>
- Ribeiro F.M. 2001. *A geometria tridimensional de falhas de empurrão investigada através de modelagem física analógica*. Thesis, Escola de Minas, Universidade Federal de Ouro Preto, Ouro Preto, 311 p.
- Richter F., Lana C., Stevens G., Buick I., Pedrosa-Soares A.C., Alkmim F.F., Cutts K. 2016. Sedimentation, metamorphism and granite generation in a back-arc region: Records from the Ediacaran Nova Venécia Complex (Araçuaí Orogen, Southeastern Brazil). *Precambrian Research*, **272**:78-100. <https://doi.org/10.1016/j.precamres.2015.10.012>
- Rosenbaum G., Li P., Rubatto D. 2012. The contorted New England Orogen (eastern Australia): New evidence from U-Pb geochronology of Early Permian granitoids. *Tectonics*, **31**. DOI: 10.1029/2011TC002960
- Sampaio A.R., Martins A.A.M., Loureiro H.S.C., Arcanjo J.B.A., Moraes Filho J.C.R., Souza J.D., Pereira L.H.M., Couto P.A., Melo R.C., Vieira Bento R., Borges V.P. 2002. *Projeto Extremo Sul da Bahia*. Salvador, Programa de Levantamentos Básicos do Brasil, Convênio CBPM/CPRM. 107 p.

- Sampaio A.R., Martins A.M., Loureiro H.C., Arcanjo J.B., Moraes-Filho J.C., Souza J.D., Pereira L.H., Couto P.A., Santos R.A., Melo R.C., Bento R.V., Borges, V.P. 2004. *Projeto Extremo Sul da Bahia: Geologia e Recursos Minerais*. Salvador, Companhia Baiana de Pesquisa Mineral. (Série Arquivos Abertos). v. 19. 52 p.
- Santos M.N., Chemale Jr. F., Dussin I.A., Martins M.S., Queiroga G., Pinto R.T.R., Santos A.N., Armstrong R. 2015. Provenance and paleogeographic reconstruction of a Mesoproterozoic intracratonic sag basin (Upper Espinhaço Basin, Brazil). *Sedimentary Geology*, **318**:40-57. <https://doi.org/10.1016/j.sedgeo.2014.12.006>
- Santos Pinto M., Peucat J.J., Martin H., Sabaté P. 1998. Recycling of the Archaean continental crust: the case study of the Gavião Block, Bahia, Brazil. *Journal of South American Earth Sciences*, **11**:487-498. [https://doi.org/10.1016/S0895-9811\(98\)00029-7](https://doi.org/10.1016/S0895-9811(98)00029-7)
- Santos R.F., Alkmim F.F. & Pedrosa-Soares A.C. 2009. A Formação Salinas, Orógeno Araçuaí, MG: História deformacional e significado tectônico. *Revista Brasileira de Geociências*, **39**:81-100.
- Silva F.C.A. & Oliveira F.J.S. 2009. Desenvolvimento de traços estruturais curvilíneos em cinturões de empurrões: visualização em modelagem física. *Revista Brasileira de Geociências*, **39**(1):138-150.
- Silva-Filho M.A., Moraes-Filho O., Gil C.A.A., Santos R.A. 1974. *Projeto Sul da Bahia*. Relatório Final. Salvador, CPRM, Folha SD.24-Y-B, 818 p.
- Silva L.C., Pedrosa-Soares A.C., Armstrong R., Noce C.M. 2011. Determining the timing of the collisional period of the Araçuaí Orogen by using high resolution U-Pb geochronology on zircon: a contribution to the history of western Gondwana amalgamation. *Geonomos*, **19**:180-197. <http://dx.doi.org/10.18285/geonomos.v19i2.53>
- Silva L.C., Pedrosa-Soares A.C., Armstrong R., Pinto C.P., Reis Magalhães J.T., Piacentini Pinheiro M.A., Santos G.G. 2016. Disclosing the Paleoproterozoic to Ediacaran history of the São Francisco craton basement: The Porteirinha domain (northern Araçuaí orogen, Brazil). *Journal of South American Earth Sciences*, **68**:50-67. <https://doi.org/10.1016/j.jsames.2015.12.002>
- Silva L.C., Pedrosa-Soares A.C., Teixeira L.R., Armstrong R. 2008. Tonian rift-related, A-type continental plutonism in the Araçuaí Orogen, eastern Brazil: New evidence for the breakup stage of the São Francisco–Congo Paleoproterozoic. *Gondwana Research*, **13**:527-537. DOI: 10.1016/j.gr.2007.06.002
- Spraggins S.A. & Dunne W.M. 2002. Deformation history of the Roanoke recess, Appalachians, USA. *Journal of Structural Geology*, **24**:411-433. [https://doi.org/10.1016/S0191-8141\(01\)00077-5](https://doi.org/10.1016/S0191-8141(01)00077-5)
- Szaniawski R., Mazzoli S., Jankowski L.S. 2017. Controls of structural inheritance on orogenic curvature and foreland basin sedimentation: Insights from the Przemyśl area, Western Carpathians. *Journal of Structural Geology*, **103**:137-150. <https://doi.org/10.1016/j.jsg.2017.09.004>
- Tull J.F. & Holm C.S. 2005. Structural evolution of a major Appalachian salient-recess junction: consequences of oblique collisional convergence across a continental margin transform fault. *GSA Bulletin*, **117**(3-4):482-499. <https://doi.org/10.1130/B25578.1>
- Uhlein A. 1991. *Transição cráton-faixa dobrada: exemplo do Cráton do São Francisco e da Faixa Araçuaí (Ciclo Brasileiro) no estado de Minas Gerais*. Aspectos estratigráficos e estruturais. Thesis, Universidade de São Paulo, São Paulo, 295 p.
- Uhlein A., Trompette R., Alvarenga C. 1999. Neoproterozoic glacial and gravitational sedimentation on a continental rifted margin: the Jequitá-Macaúbas sequence (Minas Gerais, Brazil). *Journal of South American Earth Sciences*, **12**:435-451. [https://doi.org/10.1016/S0895-9811\(99\)00032-2](https://doi.org/10.1016/S0895-9811(99)00032-2)
- Uhlein A., Trompette R., Egydio-Silva M. 1998. Proterozoic rifting and closure, SE border of the São Francisco craton, Brazil. *Journal of South American Earth Sciences*, **11**:191-203. [https://doi.org/10.1016/S0895-9811\(98\)00010-8](https://doi.org/10.1016/S0895-9811(98)00010-8)
- Uhlein A., Trompette R.R., Egydio-Silva M., Vauchez A. 2007. A glaciação sturtiana (~750 Ma), a estrutura do rifte Macaúbas-Santo Onofre e a estratigrafia do Grupo Macaúbas, Faixa Araçuaí. *Geonomos*, **15**:45-60.
- Weil A.B. & Sussman A.J. 2004. Classifying curved orogens based on timing relationships between structural development and vertical-axis rotations. In: Sussman A.J., & Weil A.B. (eds.), *Orogenic Curvature: Integrating Paleomagnetic and Structural Analysis*. Geological Society of America Special Paper, **383**:1-15.
- Weil A.B., Gutiérrez-Alonso G., Johnston S.T., Pastor-Galán D. 2013. Kinematic constraints on buckling a lithospheric-scale orocline along the northern margin of Gondwana: a geologic synthesis. *Tectonophysics*, **582**:25-49. <https://doi.org/10.1016/j.tecto.2012.10.006>
- Whisner S.C., Schmidt C.J., Whisner J.B. 2014. Structural analysis of the Lombard thrust sheet and adjacent areas in the Helena salient, southwest Montana, USA. *Journal of Structural Geology*, **69**:351-376. <https://doi.org/10.1016/j.jsg.2014.08.006>
- White L., Rosenbaum G., Allen C.M., Shaanan U. 2016. Orocline-driven transtensional basins: Insights from the Lower Permian Manning Basin (eastern Australia). *Tectonics*, **35**:690-703. DOI: 10.1002/2015TC004021
- Wilkerson M.S., Smaltz S.M., Bowman D.R., Fischer M.P., Higuera-Diaz I.C. 2007. 2-D and 3-D modeling of detachment folds with hinterland inflation: A natural example from the Monterrey Salient, northeastern Mexico. *Journal of Structural Geology*, **29**:73-85. <https://doi.org/10.1016/j.jsg.2006.07.010>
- Williams H.A., Stewart J.R., Betts P.G. 2009. Imposition of a Proterozoic salient on a Palaeozoic orogen at the eastern margin of Gondwana. *Gondwana Research*, **16**:669-686. <https://doi.org/10.1016/j.gr.2009.06.006>
- Wosniak R., Martins A., Oliveira R. 2013. *Mapa geológico da Folha Condeúba*. Bahia, CPRM-BA.

